Adsorption of β-Lactoglobulin on Thiol-Functionalized Mesoporous Silica

Laroussi Chaabane, Camille Loupiac, Frédéric Bouyer, Igor Bezverkhyy, Sarah Foley, Ali Assifaoui

Adsorption of β-Lactoglobulin on Thiol-Functionalized Mesoporous Silica

Journal:	*Langmuir*
Manuscript ID	la-2024-01099x.R2
Manuscript Type:	Article
Date Submitted by the Author:	08-Jul-2024
Complete List of Authors:	Chaabane, Laroussi; AgroSup Dijon Loupiac, Camille; AgroSup Dijon, UMR PAM équipe PAPC Bouyer, Frédéric; Laboratoire Interdisciplinaire Carnot de Bourgogne, Département Nanosciences Bezverkhyy, Igor; Universite de Bourgogne, ICB UMR5209 CNRS Foley, Sarah; Université de Franche-Comté Assifaoui, Ali; UMR PAM, Equipe PAPC, Université Bourgogne Franche-Comté

Adsorption of β-Lactoglobulin on Thiol-Functionalized Mesoporous Silica

Laroussi Chaabane[a*], Camille Loupiac[a], Frédéric Bouyer[b], Igor Bezverkhyy[b], Sarah Foley[c], Ali Assifaoui[a,d]**

[a] *Université Bourgogne Franche-Comté, Institut Agro, Université Bourgogne, INRAE, UMR PAM 1517, 21000 Dijon, France*

[b] *Laboratoire Interdisciplinaire Carnot de Bourgogne, UMR 6303 CNRS - Université de Bourgogne, BP 47 870, 21078 Dijon Cedex, France*

[c] *Laboratoire Chrono-environnement (UMR CNRS 6249), Université de Bourgogne Franche-Comté, F-25000 Besançon, France.*

[d] *Department of Pharmaceutical Technology, School of Pharmacy, Université de Bourgogne Franche-Comté, 7 Bd Jeanne d'Arc, 21079 Dijon, France*.

Corresponding authors:

*laroussichaabane92@gmail.com

**camille.loupiac@agrosupdijon.fr

ABSTRACT

SBA-15 mesoporous materials were synthesized with different pore sizes (5 and 10 nm) and thiol-functionalized groups and then characterized to describe their ability to differentially adsorb β-lactoglobulin (BLG), a globular protein with an ellipsoid shape measuring 6.9 nm in length and 3.6 nm in width. All adsorption experiments showed that the adsorption capacities of mesoporous materials for BLG were dependent of the duration of contact between the two materials (mesoporous and BLG) and the initial BLG concentration. It was also shown that the pore sizes and thiol groups of SBA-15-based adsorbents are an important factor for the BLG adsorption capacities. Among the tested adsorbents, thiol-functionalized SBA-15 with 10 nm pore size (SBA-15-SH-10) showed the highest adsorption capacity (0.560 $g.g^{-1}$) under optimal experimental conditions. Kinetics studies demonstrated that the adsorption occurs predominantly inside the pores with interactions occurring on heterogeneous surfaces. In addition, the thermodynamic parameters indicate a spontaneous and exothermic behavior of BLG adsorption process onto the thiol-functionalized SBA-15 mesoporous adsorbent. Finally, the characterization of SBA-15-SH-10 adsorbent at 308 K showed the occurrence of an oxidation reaction of the thiol groups to sulfonate groups during the adsorption process as confirmed by Raman spectroscopy. The spectra recorded after adsorption of the protein showed that this adsorption did not impact the secondary structure of the protein.

KEYWORDS: SBA-15 mesoporous, thiol functionalization, β-lactoglobulin, adsorption, modeling.

INTRODUCTION

The investigation of the biomacromolecule adsorption on solid materials is one of the most important fields in biotechnology. The discovery of mesostructured silica materials in 1992 by Kresge et al., opened a new field of research in the design of porous solids[1-3]. The potential of these silica materials for enzyme immobilization was first explored in 1996 by Diaz et *al.,*[4]. This was attributed to their specific characteristics such as large pore size, high specific surface area, and good hydrothermal stability, which enable these silica materials to adsorb a wide array of biomacromolecules. Consequently, various macromolecules including trypsin, lipases, lysozymes, and many others have been adsorbed on mesostructured silica materials belonging to the categories of Santa Barbara Amorphous (SBA) and Mobile Crystalline Material (MCM)[5-8]. Furthermore, when compared to other mesostructured silica substrates such as MCM-41 materials, SBA-15 materials exhibit thicker pore walls within the range of 3 to 6 nm, providing high hydrothermal stability, and being suitable for various applications in biotechnology[9,10]. The functionalization of these materials by either post-grafting or co-condensation methods can enhance their adsorptive properties, which could result in additional electrostatic repulsions or attractions, as well as an increased hydrophilic or hydrophobic nature between mesoporous silica materials and adsorbed biomacromolecules[11]. Tuning the surface chemistry of the pores opened new opportunities for developing mesoporous silica solids with very specific properties suitable for industrial applications such as adsorption processes, catalysis, drug delivery, or bio-sensing[12-15]. For example, Gomes et *al.,* immobilized alcohol dehydrogenase from *Saccharomyces cerevisiae* (ADH) on SBA-15 mesoporous materials with varying pore sizes, approximately 6.8 and 10 nm. The results showed that the adsorption enzyme penetrated deeper into the pores and exhibited good reusability[16]. Moreover, Miao et *al.,* modified SBA-15 with hydrophobic and hydrophilic molecules such as 3-aminopropyltriethoxysilane (APTS) and 3-glycidyloxypropyltrimethoxysilane (GPTMS), respectively, to study the immobilization of

myoglobin[17]. Their funding demonstrated that the loading yields of myoglobin by SBA-15-APTS and SBA-15-GPTMS were 511 and 548 $mg.g^{-1}$, respectively, compared to only 396 $mg.g^{-1}$ with native SBA-15[17]. The key is that surface-macromolecule interactions can be improved by immobilizing the protein on such "inorganic-organic materials". Nevertheless, there are currently no studies assessing the effects of surface functionalization with thiol groups on the kinetics and adsorption properties of proteins or peptides through their thiolate groups, originating from cysteins.

Several studies have described in detail the structure of β-lactoglobulin (BLG), a globular protein from milk whey. At pH 7, the protein is in a dimer form with a molecular weight (M_w) of 36.8 kDa[18-20]. The BLG contains two disulfide bridges (Cys66-Cys160 and Cys106-Cys119) and a free thiolate group (Cys121), which are inaccessible to polar medium in the native state of the protein because these groups are in a hydrophobic pocket[21-23]. In addition to the disulfide bridges, hydrophobic, hydrogen bonds, and ionic interactions between peptide chains contribute to stabilizing the protein's conformation. Belonging to the lipocalin family, the secondary structure of the BLG is mainly constituted of beta-sheet, classifying it as a hard protein. X-ray crystallography and small-angle X-ray scattering studies have revealed that dimeric conformation of BLG is an approximately prolate ellipsoid, measuring 6.9 nm in length and 3.6 nm in width. Alternatively, the dimer can be described by two impinging spheres (monomers) each with a radius of 1.8 nm[24].

Despite these advances, there is a notable gap in the research regarding the effects of surface functionalization with thiol groups on the kinetics and adsorption properties of proteins or peptides through their thiolate groups, originating from cysteins. This study aims to address this gap by examining the influence of pore size and thiol group functionalization on SBA-15 materials on the adsorption yield of BLG, a globular protein from milk whey.

Furthermore, to highlight the effect of functionalization of SBA-15 materials on BLG adsorption, the effects of contact time, BLG concentration, and temperature on the equilibrium adsorption capacities of the adsorbents were studied and compared. To understand the mechanism of the adsorption process, pseudo-first-order, pseudo-second-order, Elovich, and Bangham's models were fitted to experimental kinetic data. Furthermore, the Freundlich, and Langmuir approaches were applied to analyze the adsorption data. The thermodynamic parameters of the protein adsorption at various temperatures were also systematically calculated and compared from the experiments carried out between 278 and 308 K. We also used Raman spectroscopy to better understand the effect of the adsorption of the protein on the functionalized mesoporous materials but also on the structure of the proteins.

MATERIALS AND METHODS

Chemicals and reagents

Pluronic triblock copolymer (P123, $(EO)_{20}(PO)_{70}(EO)_{20}$, M_w= 5800 g.mol^{-1}, Aldrich), tetraethylorthosilicate (TEOS, Aldrich), (3-mercaptopropyl)-triethoxysilane (MPTES, Fluorochem), hydrochloric acid (HCl, Fisher Chemicals, 38%), citric acid ($C_6H_8O_7$, Aldrich, ≥99.0 %), sodium phosphate dibasic (Na_2HPO_4, Aldrich, ≥99.0 %) sodium chloride (NaCl, Aldrich, ≥99.0 %), trichloroacetic acid (Serva, Heidelberg, Germany, ≥99.0%) were used as received. Anhydrous toluene (Aldrich, 99.8%) was pre-dried over 4 Å activated molecular sieves and stored in a tube schlenk before use.

β-lactoglobulin (BLG) was purified from whey powder (Bipro, Davisco, Geneva, Switzerland) following the method of Fox et *al.*[25]. The powder was slowly dissolved in water (73.5 g of whey powder/L) under constant agitation for at least 2 h. Trichloroacetic acid was used as a precipitant (3.1 g in 20 mL water per 100 mL of protein solution). The mixture was centrifuged at 10 000 g for 30 min at 20 °C and the supernatant was dialyzed (cutoff of the

dialysis membrane 3500 Da) under constant stirring deionized water and 3 times for 2 h against sodium chloride solution at 0.1 M. Absorbance of the diluted protein was measured by UV-visible spectroscopy in the range of 220-350 nm. The protein's concentration was determined using the absorbance intensity at 278 nm and ε (0.1%) = 0.96 L. $cm^{-1}.g^{-1}$. The final concentration of purified BLG was around 20 $g.L^{-1}$. After purification, the protein was freeze-dried, and the resulting powder was stored at -20 °C until use. To prepare the mother solution of the BLG ([BLG]: 32.7 $g.L^{-1}$) used for the adsorption experiments, the powder was slowly resuspended in a Mc Illvaine buffer (0.2 M Na_2HPO_4 and 0.1 M citric acid) at pH 7 and dialyzed against the buffer (3 times x at least 2h) 24 h before use.

Mesoporous Materials: Structural Characterization's

The functionalized and as-synthesized materials were characterized by Fourier Transform-Infrared Spectroscopy (FTIR) using a Bruker Equinox 55 spectrometer equipped with a DTGS detector. The FTIR spectra were recorded using KBr pellets prepared by mixing a small amount of material (~1-2 mg) with 200 mg of KBr. Each sample was scanned 100 times between 4000 cm^{-1} to 400 cm^{-1} with a resolution of 4 cm^{-1}.

The thermal decomposition of organic moieties grafted onto the SBA-15 materials was characterized by TGA (Mettler Toledo, USA). The samples were dried at 100°C for 1 h and heated under air flow between 100 °C and 800 °C with a heating rate of 10 $°C.min^{-1}$.

The mesoporous structure of the SBA-15 materials was inspected by Transmission Electron Microscopy (TEM, JEM2100, JEOL; Japan).

The X-ray Photo-electron Spectroscopy (XPS) analysis were achieved using a spectrometer (Thermo Fisher Scientific, USA) with a monochromatized K_α-Al radiation (1486.7 eV), and an X-ray power of 450 W. The carbon C1s peak at 285 eV was considered as a reference. The core level characteristic peaks for O1s, Si2s, and S2s were measured.

The structural organization of the mesoporous materials was performed using low-angle Powder X-Ray Diffraction patterns (PXRD) collected on an X-ray diffractometer (Bruker D8, USA) with Cu K_α radiation. The tube voltage was 35 kV, and the current was 35 mA.

The specific surface area (S_{BET}), pore size (Dp), and pore volume (V_m) of the non-functionalized and functionalized SBA-15 materials were measured by N_2 adsorption/desorption on a Micromeritics ASAP 2020 setup (Micromeritics Instrument, Nocross, GA). All samples were previously degassed at 80 °C under N_2 flow for 24 h prior to analysis. Specific surface areas (S_{BET}) were calculated according to Brunauer-Emmett-Teller (BET) equation at a relative pressure ranging from 0.06 to 0.25 and the pore size distribution (D_p) was obtained the adsorption branch of isotherms using the Barrett-Joyner-Halenda (BJH) approach. The pore volume was calculated from the amount of adsorbed N_2 at P/P_0= 0.95.

The Raman spectroscopy includes a Spectra Physics Nd/YAG laser model LAB-170-10 which delivers pulses with a duration of 5 ns at a repetition rate of 10 Hz. The equivalent power density at the sample was 30 mW mm^{-2} for a beam diameter of 1 cm. The spectra were recorded using the second harmonic emission wavelength (532 nm) of the laser. The scattered light was detected at 90° using a Princeton Instruments spectroscopy system, which includes an Acton Spectra Pro 2500i monochromator with maximum resolution of 0.035 nm and a PIMAX-1024-RB CCD camera. The spectral resolution of the system was 7 cm^{-1} as determined by the FWHM of the Raman spectrum of N_2 in air.

Synthesis of the SBA-15-OH mesoporous materials

Pristine SBA-15-OH mesoporous materials with two different pore sizes (5 nm and 10 nm) were synthesized based on the method developed by Zhao *et al.,*[26] and adapted by Gustafsson *et al.,*[27]. In the typical synthesis, mesoporous materials were denoted SBA-15-OH-

5 and SBA-15-OH-10, which reflects the measured average pore size 5 nm and 10 nm, respectively.

4.0 g of Pluronic P123 was dissolved in 80 mL of hydrochloric acid solution (HCl, 2 M) and the mixture was vigorously stirred for 2 h at 40 °C. After that, 6.24 g of TEOS was added, and the solution stirred at the same temperature for an additional 24 h. The gel mixture was aged in a Teflon-lined stainless-steel autoclave for another 24 h at 100 °C or 130 °C to prepare SBA-15-OH-5 and SBA-15-OH-10 materials, respectively. At the end of the condensation process, the solid precipitate was recovered by centrifugation (10 000 g, 10 min, 20 °C), washed with deionized water until the conductivity was close to that of deionized water, and air-dried at room temperature for 2 days. Finally, the template was removed from the white product by calcination in air at 550 °C for 6 h.

Post-grafting of SBA-15-OH-5 and SBA-15-OH-10 materials

The functionalization of SBA-15-OH-5 and SBA-15-OH-10 mesoporous materials with thiol groups using a post-grafting method was performed using the previously reported methods with some modifications[28]. First, 200 mg of SBA-15-OH-5 or SBA-15-OH-10 materials were dried at 373 K for 8 h to remove physiosorbed water. Afterward, the synthesized mesoporous silica was dispersed in 10 mL of anhydrous toluene under N_2 flow. Then, 8.5 mmol MPTES was added dropwise into the synthesized mesoporous silica (SBA-15-OH-5 or SBA-15-OH-10) materials and the mixture was stirred under reflux at 353 K for 24 h. At the end of the reaction, the functionalized samples were recovered by centrifugation (10 000 *g*, 20 min, 293 K), washed with ethanol several times to remove the unreacted and physically adsorbed reagents, and dried under vacuum at 353 K overnight. The samples functionalized with MPTES were marked as SBA-15-SH-5 and SBA-15-SH-10.

Adsorption studies

The adsorption capacities of β-lactoglobulin (BLG) onto SBA-15-based adsorbents were examined in McIlvaine buffer solutions (0.2 M Na_2HPO_4 and 0.1 M citric acid) at pH= 7. Three parameters (contact time, initial BLG concentration and temperature) were studied. For a typical experiment, 50 mg of adsorbent (SBA-15-OH-5, SBA-15-OH-10, SBA-15-SH-5, or SBA-15-SH-10) were added to a 10 mL amber glass bottle containing 4 mL of the BLG solution ([BLG]=9.0 $g.L^{-1}$). The suspension was mixed at 298 K using an incubator orbital shaker at 120 rpm for various contact times to study the kinetics of the different SBA-15-based adsorbents. BLG proteins adsorption capacities were examined over a time range of 30 to 3600 minutes at 298 K. In addition, the initial β-lactoglobulin (BLG) concentrations used for adsorption isotherm studies ranged from 1 to 11 $g.L^{-1}$ and were examined at four different temperature conditions (278, 288, 298, and 308 K). After each experiment, the supernatant was separated by centrifugation at 4 500 g for 5 minutes and then filtered through a syringe filter with a 0.2 µm pore size. The pellet was washed three times for 15 minutes with 1 mL of McIlvaine buffer solution (pH=7). Finally, the initial and equilibrium BLG concentration in each solution were determined using a UV-Visible spectrophotometer at a detection wavelength of 278 nm.

The adsorption capacity Q_e ($g.g^{-1}$) at the equilibrium was calculated by the following equation:

$$Q_e = \frac{V(C_0 - C_e)}{m} \quad (\mathbf{1})$$

where C_0 ($g.L^{-1}$) is the initial concentration of BLG, C_e ($g.L^{-1}$) is the concentration of BLG at equilibrium, V (L) is the volume of the adsorbent and m (g) is the mass of the adsorbent.

For the kinetic study of BLG adsorption on the SBA-15-based adsorbents, the adsorption capacity Q_t ($g.L^{-1}$) at a time t was calculated using **Eq. (2)**:

$$Q_t = \frac{V(C_0 - C_t)}{m} \quad (2)$$

where C_t ($g.g^{-1}$) is the residual BLG concentration in solution at time t.

RESULTS AND DISCUSSION

Structural characterizations of SBA-15 materials after synthesis and functionalization.

Fig.1 presents the N_2 isotherms and the pore size distribution of the both the native and functionalized materials. For all samples, the adsorption/desorption curves **(Fig. 1A)** exhibit type IV isotherms with the H1 hysteresis according to the IUPAC classification, which is typical of mesoporous materials.

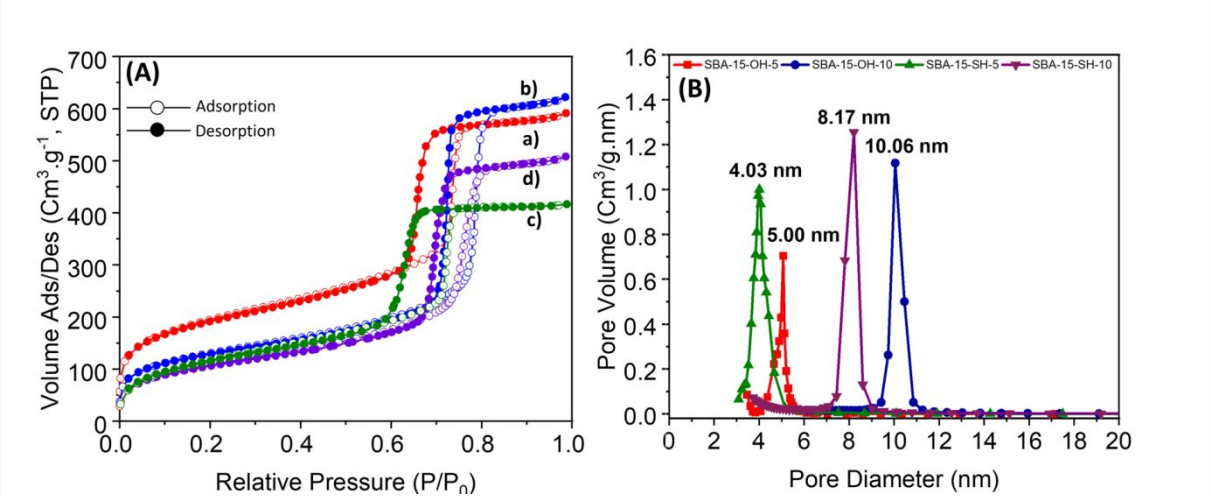

Fig. 1. (A) N_2 adsorption -desorption isotherms at 77 K and **(B)** Pore size distribution of **(a)** SBA-15-OH-5**, (b)** SBA-15-OH-10, **(c)** SBA-15-SH- and **(d)** SBA-15-SH-10.

Moreover, the hydrothermal temperature has a significant effect on the specific surface area (S_{BET}), pore volume (Vp), pore size (Dp), and pore wall thickness (t_{wall}) of the non-functionalized SBA-15 materials (SBA-15-OH-5 and SBA-15-OH-10). This effect is evident as the adsorption-desorption loop shifts to the right leading to an increase in pore size. As the hydrothermal temperature increases, the specific surface areas increase from the 698 $m^2.g^{-1}$ at 373 K to 702 $m^2.g^{-1}$ at 403 K for SBA-15-OH-5 and SBA-15-OH-10, respectively **(Table S1)**. According to the Barret-Joyner-Halenda (BJH) model method, the pore size (Dp) of the non-functionalized SBA-15 materials increases from 5 nm to about 10 nm with increasing temperature from 373 K to 403 K, respectively. However, for the thiol-functionalized SBA-15 mesoporous materials (SBA-15-SH-5 and SBA-15-SH-10), we observed **(Table S1)**, a decrease in the specific surface area (S_{BET}), suggesting the successful loading of mercaptopropyl groups into the pores. This interpretation was also confirmed by the lower pore volume (Vp) and pore size (Dp) of thiol-functionalized SBA-15 materials, which demonstrated that thiol-functionalized groups occupied part of pore space and mainly covered the inner surface of mesoporous channels **(Table S1)**.

The unit cell parameters (a_0) and the d_{100} values, summarized in **Table S1**, were calculated from the small-angle X-ray diffraction patterns of SBA-15-based materials **(Fig. S1)**. The non-functionalized SBA-15 materials (SBA-15-OH-5 and SBA-15-OH-10) revealed three well-resolved peaks, denoted as (100), (110), and (200) reflections. These peaks are characteristics of hexagonal symmetry (P6mm) with highly well-ordered mesoporous structure, as discussed by Miao et *al.,*[29]. In the same situation, the thiol-functionalized SBA-15 mesoporous materials (SBA-15-SH-5 and SBA-15-SH-10) also maintained an intense (100) peak and weaker (110) and (200) peaks. This observation further confirmed that both SBA-15-SH-5 and SBA-15-SH-10 materials maintained a hexagonally ordered structure after functionalization. In addition, the larger wall thickness (t_{wall}) and the smaller pore size of

functionalized materials compared to the non-functionalized materials confirmed the presence of the mercaptopropyl groups grafted inside the mesopore channels, which influences both the hexagonal symmetry and pore size.

The mesoporous structure of the non-functionalized SBA-15 materials (SBA-15-OH-5 and SBA-15-OH-10) were investigated using transmission electron microscopy (TEM). **Figs. S2a and S2c** show that the SBA-15-OH-5 and SBA-15-OH-10 materials consist of parallel pore channels and highly ordered mesopores. Consequently, the qualitative studies demonstrate that the non-functionalized SBA-15 materials possessed a large-scale hexagonal structure. Additionally, the TEM images revealed that the diameter of the pore channel was 4.9 nm and 10.0 nm for SBA-15-OH-5 and SBA-15-OH-10, respectively, which confirmed the results of the small-angle XRD patterns, as well as the narrow pore size distribution determined by N_2 adsorption-desorption isotherms **(Fig. 1B)**.

FTIR spectroscopy was used to further confirm the presence of thiol groups on the functionalized SBA-15 mesoporous materials (SBA-15-SH-5 and SBA-15-SH-10). It can be seen from **Fig. S3** that all the samples display similar characteristic bands of silica network, along with absorbance bands in the range 454-479 cm^{-1} and 1074-1077 cm^{-1}. These bands are assigned to the symmetric and asymmetric stretching vibration of Si-O-Si bands, respectively. Additionally, the presence of adsorption bands located in the range 1630-1632 cm^{-1}, and 3435-3517 cm^{-1} are attributed to O-H bending vibration of physically adsorbed moisture and O-H stretching vibration of hydrogen-bonded silanol groups, respectively[30].

After functionalization of mercaptopropyl groups onto the SBA-15-OH-5 **(Fig. S3a)** and SBA-15-OH-10 **(Fig. S3b)** materials, the intensity of the absorption bands located in the range 808-825 cm^{-1} indexing to the stretching vibration of free silanol groups (Si-OH) were decreased for SBA-15-SH-5 and SBA-15-SH-10 **(Fig. S3c and Fig. S3d)**, suggesting the grafting of organosilanes with silanol groups (-OH) was efficient. Meanwhile, the presence of

novel absorption bands appeared in the range of 2891-3007 cm^{-1}, which were due to the C-H stretching vibrations in $-CH_2$ and $-CH_3$, indirectly confirmed that MPTES has successfully grafted onto the SBA-15-OH-5 and SBA-15-OH-10 materials. Moreover, a weak stretching vibration of -SH groups also showed in the range 2570-2670 cm^{-1}, confirming that MPTES was successfully grafted on the silica surface (**See Fig. S4**).

XPS analysis can identify the surface composition of the thiol-functionalized SBA-15 mesoporous materials. XPS results (**Fig. S5**) show that the surface of the SBA-15-SH-5 and SBA-15-SH-10 materials contained only Si, O, C, and S. In all cases, the presence of two peaks around 163 and 230 eV, corresponding to S2p and S2s were observed, which are characteristic of thiol groups on the silica surface, and this confirmed the absence of oxidation of thiol groups to sulfonate groups during the post-grafting process.

The thermal stability of the non-functionalized and thiol-functionalized SBA-15 mesoporous materials were also evaluated by thermogravimetric analysis (TGA) from 50 °C to 800 °C under airflow. As shown in **Fig. S6**, thermogravimetric analysis curves for SBA-15-OH-5 and SBA-15-OH-10 show a slight weight loss between 200 °C and 800 °C, of about 1.0 % wt. and 1.2 % wt., respectively, due to the dehydroxylation of silica and organic components completely removed after calcination treatment. The weight losses lower than 200 °C from the thiol-functionalized SBA-15 mesoporous materials were mainly attributed to the evaporation of the adsorbed water after heating, while these weight losses at the higher temperature were ascribed to the thermal degradation of grafted organic groups. In addition, the grafting densities of the SBA-15-SH-5 and SBA-15-SH-10 mesoporous materials were calculated, i.e. 1.45 $mmol.g^{-1}$ and 2.16 $mmol.g^{-1}$, respectively **(Table S2)**.

β-lactoglobulin (BLG) adsorption onto the mesoporous materials

Influence of contact time on the adsorption capacities

To understand the adsorption behaviors of BLG towards the various mesoporous materials, experiments were carried out at different contact times in the range of 30-3600 minutes (**Fig. 2**) and the initial concentration used was 9 $g.L^{-1}$ (0.49 mM).

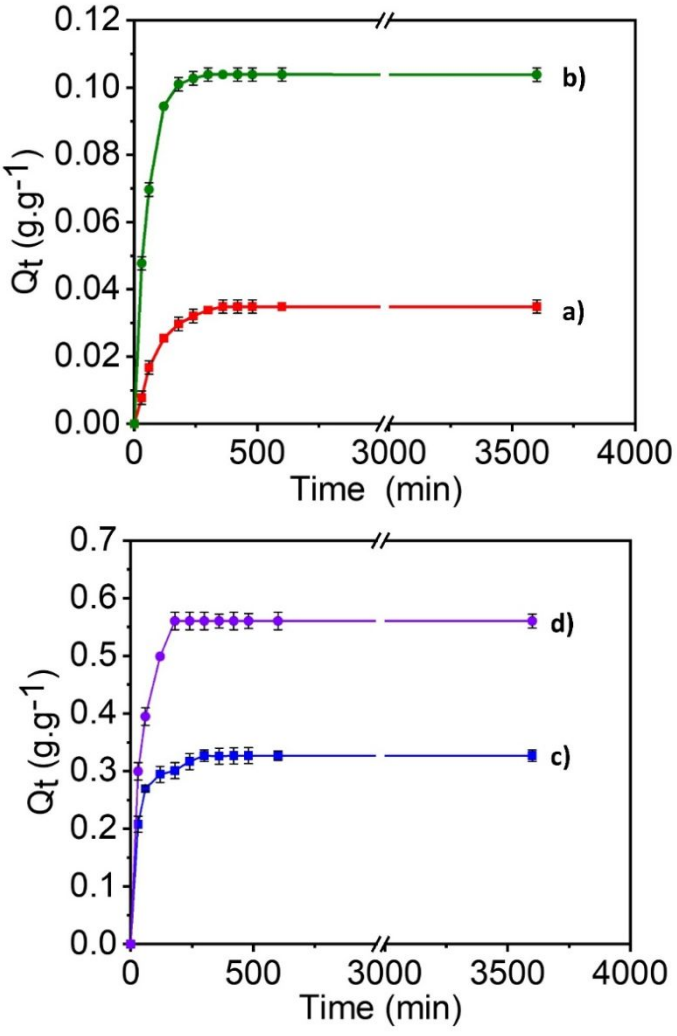

Fig. 2. Influence of contact time on the adsorption of BLG by **(a)** SBA-15-OH-5, **(b)** SBA-15-SH-5, **(c)** SBA-15-OH-10, and **(d)** SBA-15-SH-10. **Experimental conditions**: [BLG] =

9.0 g.L^{-1}, [Adsorbent]= 12.5 g.L^{-1}, pH = 7, and T = 298 K. The error bars correspond to one standard deviation n = 2.

Fig. 2 shows that the adsorption capacity of BLG on the adsorbents, as a function of the contact time, have the shape of the saturation curves. In all cases, BLG is adsorbed onto the mesoporous materials, probably due to the availability of high surface area, pore size, and available adsorption sites (OH groups for native SBA-15-OH and both OH and SH groups for functionalized materials).

Furthermore, the time required to achieve equilibrium depends on the average pore size and the functional groups: 360, 300, 240 and 180 minutes for SBA-15-OH-5, SBA-15-SH-5, SBA-15-OH-10, and SBA-15-SH-10, respectively. It is noteworthy that the time needed to reach equilibrium is longer for SBA-15-OH-5 compared to SBA-15-OH-10, as BLG molecules diffuse slowly in the smaller pores. The functionalization of mercaptopropyl groups onto the SBA-15-OH-5 and SBA-15-OH-10 materials resulted in higher adsorption capacities for BLG proteins. In addition, the SBA-15-SH-10 adsorbent can achieve equilibrium adsorption faster than SBA-15-SH-5 adsorbent with the highest adsorption capacity of BLG proteins (0.56±0.01 g.g^{-1}) which correspond to 30 µmol of BLG per gram of SBA-15-SH-10. This can be attributed to the greater abundance and accessibility of thiol groups onto SBA-15-SH-10, as well as the higher grafting density of thiol-silane groups (2.16 mmol.g^{-1} compared to 1.45 mmol.g^{-1} for the SBA-15-SH-5, see **Table S2**).

Influence of initial BLG concentrations on the adsorption capacities of the mesoporous materials

To further investigate the adsorption behavior of BLG on the mesoporous materials, different initial concentrations of BLG ranging from 1 to 11 g.L^{-1} were studied at a fixed contact time of 24 hours (**Fig. 3**).

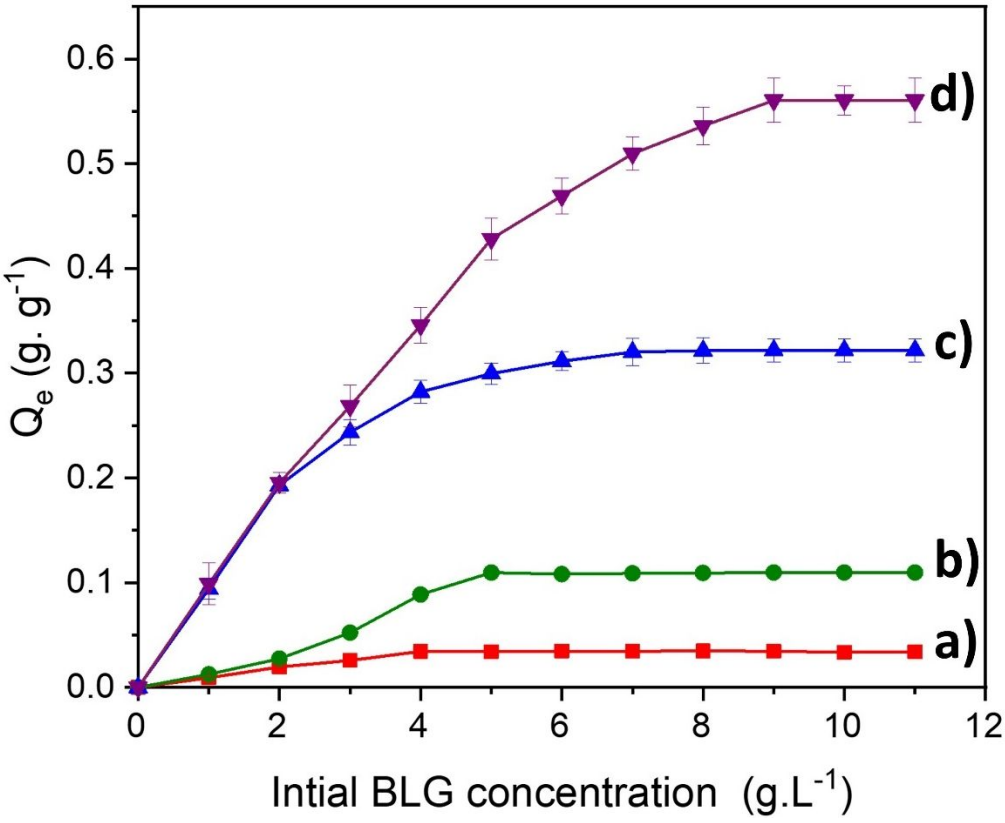

Fig. 3. Influence of initial concentration of BLG on their absorptions by **(a)** SBA-15-OH-5, **(b)** SBA-15-SH-5, **(c)** SBA-15-OH-10, and **(d)** SBA-15-SH-10. **Experimental conditions**: [Adsorbent] = 12.5 g.L^{-1}, contact time = 24 h, pH = 7, and T = 298 K. The error bars represent one standard deviation (n = 2).

Fig. 3 shows that the equilibrium adsorption capacities (Qe) of adsorbents increase with increasing the initial BLG concentration rises and eventually reach a plateau. For materials with the same pore size, the adsorption capacity is nearly the same at low initial BLG concentrations. Upon reaching the saturation point of the adsorbent surfaces, the maximum adsorption capacities ($Q_{e,max}$) of BLG proteins at the plateau, are measured as 0.03±0.01, 0.10±0.01, 0.33±0.01, and 0.56±0.01 g.g^{-1} for SBA-15-OH-5, SBA-15-SH-5, SBA-15-OH-10, and SBA-15-SH-10, respectively. These results confirm that the SBA-15-SH-10 adsorbent exhibits the highest adsorption capacity towards BLG proteins. It is important to note that the equilibrium adsorption capacities of the mesoporous materials become nearly constant when the initial

concentration of BLG is close to 9.0 $g.L^{-1}$ due to the saturation of the active adsorption sites on the surface of the adsorbents. For subsequent experiments, this concentration (9.0 $g.L^{-1}$) will be used.

Modelization of the adsorption kinetics of β-lactoglobulin (BLG) onto the different mesoporous materials

To better describe the mechanism of adsorption of BLG proteins onto SBA-15 adsorbents as well as on diffusion processes, pseudo-first-order (PFO), pseudo-second-order (PSO), Elovich, and Bangham's kinetics models were applied to the experimental data previously discussed.

The pseudo-first-order kinetic (PFO) model assumes that the adsorption is controlled by diffusion step and the rate of adsorption is proportional to the difference between the quantity adsorbed at equilibrium (Q_e) and the quantity (Q_t) adsorbed at a given time. Additionally, it assumes that the adsorption is reversible. **Equation 3** describes the linear form of the PFO model[31]:

$$\log(Q_e - Q_t) = \log Q_e - \frac{k_f}{2.303} t \quad \textbf{(3)}$$

where Q_e and Q_t ($g.g^{-1}$) are the adsorption capacities at time (t) and at equilibrium, respectively, and k_f (min^{-1}) is the rate constant. The values of Q_e and k_f are calculated respectively from the intercept and the slope of the linear plot of $\log(Q_e\text{-}Qt)$ as a function of the time.

The pseudo-second-order (PSO) model is often used successfully to describe the mechanism of the fixing of an adsorbate onto the surface of an adsorbent. The linear form of the PSO model is given by **Eq. 4**[32]:

$$\frac{t}{Q_t} = \left(\frac{1}{k_s Q_e^2}\right) + \frac{t}{Q_e} \quad \textbf{(4)}$$

where k_s (g.mmol^{-1}.min^{-1}) is the rate constant adsorption of PSO model. The values of ks and Q_e are calculated from the intercept ($1/k_sQ_e^2$) and the slope ($1/Q_e$) of the linear plot of t/Q_t as a function of the time.

Another interesting model to describe the adsorption process of BLG on the heterogeneous surface of the SBA-15-based adsorbents is the Elovich or Roginsky-Zeldovich kinetic model and is described by **Eq. 5**[33]:

$$Q_t = \frac{1}{B}\ln(t) + \frac{1}{B}\ln(AxB) \quad \textbf{(5)}$$

where A (mmol.g^{-1}.min^{-1}) and B (g.mmol^{-1}) are the Elovich initial adsorption rate and the desorption constants, respectively. The values of A and B are determined from the slope and the intercept of the linear plots of Q_t as a function of ln(t).

The Bangham's model was used to examine whether pore diffusion was the sole controlling step in the adsorption process or not. Equation 6 describes the linear form of the Bangham's model [34, 35]:

$$\log[\log\left(\frac{C_0}{C_0 - Q_t\, m}\right)] = \log\left(\frac{k_A\, m}{2.303\, V}\right) + \alpha \log t \quad \textbf{(6)}$$

where C_0 (g.L^{-1}) is the initial concentration of adsorbate in the solution, Q_t is the adsorption capacity at time t, V (L) is the volume of the solution, m (g) is the weight of adsorbent, and α and k_A (L.g^{-1}.L^{-1}) are constants.

In order to estimate the most appropriate model to describe the adsorption kinetic process, the calculated expressions of some error functions including the correlation coefficient (R^2) and the standard deviation $\Delta_{q\_}$(%) are:

$$R^2 = \frac{\Sigma(Q_{t,\,cal} - \overline{Q}_{t,exp})^2}{\Sigma(Q_{t,\,cal} - \overline{Q}_{t,exp})^2 + \Sigma(Q_{t,\,cal} - Q_{t,exp})^2} \quad \textbf{(7)}$$

$$\Delta_q(\%) = \sqrt{\frac{\Sigma(\frac{Q_{t,\,exp}-Q_{t,cal}}{Q_{t,\,exp}})^2}{(n-1)}} \times 100 \quad \textbf{(8)}$$

where $Q_{t,exp}$ and $Q_{t,cal}$ ($g.g^{-1}$) are the experimental and calculated adsorption capacities at time t, respectively, $\overline{Q}_{t,exp}$ is the average of $Q_{t,exp}$, and n is the number of data points.

The evaluation of the kinetic parameters obtained from the linear fittings of PFO, PSO, Elovich models are presented in **Table S3** together with the error functions of the correlation coefficient (R^2) and the standard deviation Δ_q (%). **Fig. 4** compares the experimental data and the data coming from these kinetics models, where the parameters were established from linear regression for the SBA-based adsorbents.

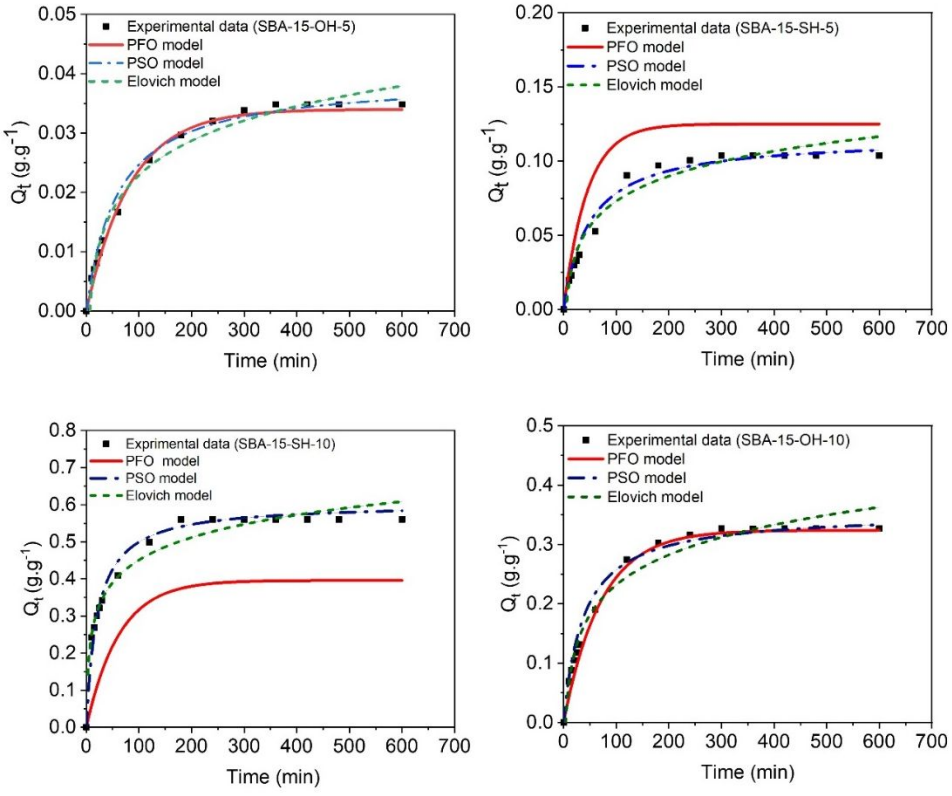

Fig. 4. Comparison of experimental and predicted kinetics of BLG adsorption onto the SBA-15-OH-5, SBA-15-OH-10, SBA-15-SH-5, and SBA-15-SH-10 mesoporous adsorbents, according to the pseudo-first-order (PFO), the pseudo-second-order (PSO), and the Elovich models.

The curves suggest that the pseudo-first-order (PFO) model is more appropriate than the pseudo-second-order (PSO) model to fit the experimental adsorption data for the SBA-15-OH-5 and SBA-15-OH-10 adsorbents. This conclusion is supported by the higher values of correlation coefficient (R^2) and the smaller values of the standard deviation Δq (%) (**Table S3**). In contrast, the experimental adsorptions of BLG proteins onto SBA-15-SH-5 and SBA-15-SH-10 are well fitted by the PSO model considering that the experimental data ($Q_{e,exp.}$, $g.g^{-1}$) are much closer to the calculated equilibrium adsorption capacity ($Q_{e,calc.}$, $g.g^{-1}$). Furthemore, the SBA-15-SH-10 adsorbent exhibits a higher adsorption rate constant (k_s) than SBA-15-SH-5 adsorbent. This behavior can be attributed to the higher grafting density of thiol groups and the larger pore diameter.

The Elovich model was then employed to attain a better understanding of the adsorption process when the adsorbent's surface is heterogeneous, and the adsorption activation energy is non-uniform[36]. The parameters and adjustments of the Elovich model used are shown in **Table S3** and **Fig. 4.** The higher correlation coefficient (R^2) of the Elovich model ($R^2 > 0.942$) for the SBA-15 adsorbents allow us to conclude that the surfaces of the adsorbents are heterogeneous, with a greater heterogeneity observed on the surface of the SBA-15-SH-10 adsorbent. Furthermore, the initial adsorption rate constant "A" increases in the order SBA-15-OH-5 < SBA-15-SH-5 < SBA-15-OH-10 < SBA-15-SH-10. In contrast, the desorption constant "B" decreases in the order SBA-15-OH-5 > SBA-15-SH-5 > SBA-15-OH-10 > SBA-15-SH-10. This behavior may be attributed to the higher affinity of BLG proteins towards the heterogeneous active adsorption sites on functionalized materials between two disulfide bridges (Cys66-Cys160 and Cys106-Cys119) in BLG proteins and thiolate groups on SBA-15-based materials, or electrostatic and hydrogen bonds interactions, along with diffusion into the pores of the adsorbents.

The Bangham's kinetic model was found to describe the ability of BLG proteins to be adsorbed within the pores of SBA-15-based adsorbents. The values of the Aharoni's parameters (k_A and α) as well as R^2 and Δq (%) values, are given in **Table S4** and the corresponding linear plots are displayed in **Fig. 5**.

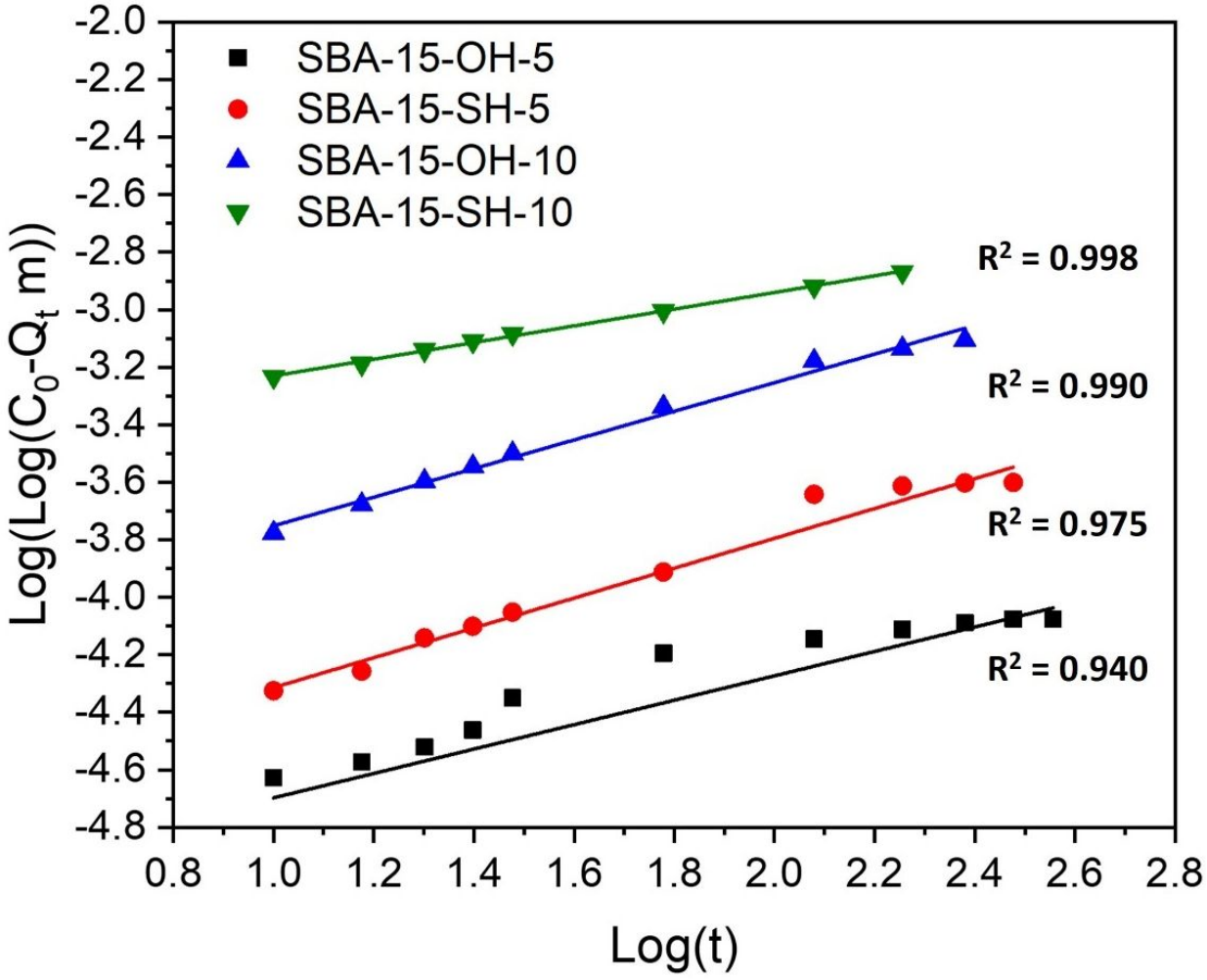

Fig. 5. Bangham's kinetic plots for the adsorption of BLG proteins onto SBA-15-OH-5, SBA-15-SH-5, SBA-15-OH-10, SBA-15-SH-10.

Based on the best correlation coefficient values (R^2~1) obtained from the Bangham's kinetic model, it can be inferred that the adsorption of BLG proteins occurs through diffusion into the pores of the SBA-15-OH-10 and SBA-15-SH-10 adsorbents.

This observation is consistent with the conditions used in this study, as the dimeric form of BLG protein is ellipsoidal with a unit cell of a= 2.9, b= 3.4, and c= 8.0 nm[37, 38], which is larger than the SBA-15-OH-5, and SBA-15-SH-5 entrance sizes (pore diameter= 5.00 and 4.03 nm, see **Table S1**). Consequently, it has a reduced chance of entering these smaller pores, leading to hindered diffusion inside them. Furthermore, the diffusion constant k_A decreases according in the following order: SBA-15-SH-5 > SBA-15-OH-5, and SBA-15-SH-10 > SBA-15-OH-10. This ranking clearly exhibits that the diffusion constants depend on both the pore size and the grafting density of the thiol groups on the surface SBA-15-based adsorbents. Moreover, the low values of rate constants α (about α <1 for SBA-15-OH-10 and SBA-15-OH-5) provide evidence that pore diffusion was the predominant mechanism during the adsorption process of BLG proteins.

Modeling of the adsorption isotherms of BLG onto mesoporous materials

Several isotherms' models can be used to determine the nature of adsorption (chemical or physical) and the surface properties of the adsorbent (heterogeneous or homogeneous surface) [39]. For this study, the Langmuir and Freundlich models were employed to explore the effect of temperature on the adsorption process of SBA-15 adsorbents. The Langmuir isotherm model is widely used to describe a monolayer adsorption environment, assuming that the adsorption surface is homogeneous and that there are no interactions and steric hindrances among the adsorbates[40, 41]. The linear form of the Langmuir isotherm model is expressed by **Eq. (9)**:

$$\frac{C_e}{Q_e} = \frac{C_e}{Q_{max}} + \frac{1}{b\,Q_{max}} \quad \textbf{(9)}$$

where Q_{max} (g.g^{-1}) is the maximum monolayer adsorption capacity and b (L.g^{-1}) is a Langmuir constant. The values of b and Q_{max} are obtained from the slope and the intercept of the linear plot of C_e/Q_e vs. C_e.

The Freundlich isotherm is an empirical model for reversible adsorption on rough and heterogeneous surfaces with interaction between the adsorbates. The linear form of the Freundlich isotherm model is given as by **Eq. (10)**[42]:

$$\ln Q_e = \ln(K_F) + \frac{1}{n}\ln(C_e) \quad \textbf{(10)}$$

where K_F ($(g.g^{-1})(g.L^{-1})^{1/n}$) is Freundlich isotherm constant, and n (a dimensionless parameter) is the exponential constant of the Freundlich model related to adsorption intensity which is favorable when $1/n < 1$. The values of K_F and $1/n$ are obtained from the slope and the intercept of the linear plot of $\ln(Q_e)$ vs. ln(Ce).

The fitted graphs of the Langmuir and Freundlich isotherm models are presented in **Fig. 6**, and the corresponding numerical parameters for both models are gathered in **Table S5** and **Table S6**.

The adsorption capacities of BLG proteins onto the SBA-15-OH-5 and SBA-15-OH-10 adsorbents exhibited an increase as the solution temperature increased (**Fig. 6**). Surprisingly, the adsorption capacities of BLG proteins onto the SBA-15-SH-5 and SBA-15-SH-10 adsorbents significantly decreased with rising temperatures, indicating a potentially low interaction between the active sites of adsorbents and the BLG proteins. These results suggest that the behavior of thiol groups present on the adsorbents varies with temperature when interacting with BLG proteins.

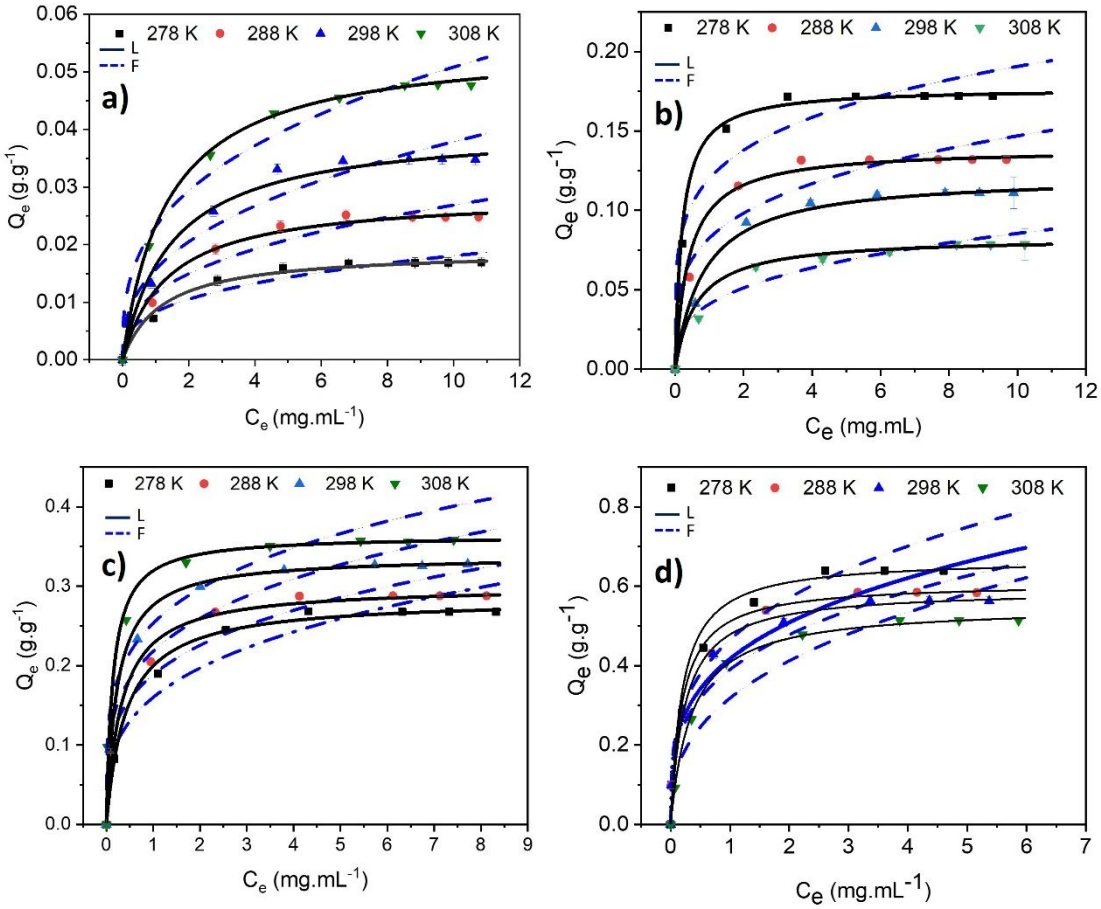

Fig. 6. Comparison of the predicted adsorption isotherms and the experimental adsorption data for BLG proteins onto **(a)** SBA-15-OH-5, **(b)** SBA-15-SH-5, **(c)** SBA-15-OH-10, and **(d)** SBA-15-SH-10 adsorbents at 278, 288, 298, and 308 K, according to the Langmuir **(L)** and Freundlich **(F)** isotherm models.

It was also observed that the Langmuir model provided a better fit for the adsorption data compared to the Freundlich model, as evidenced by the higher values of correlation coefficient (R^2) and the least values of standard deviation Δq (%) (**Fig. 6** and **Tables S5-6**). Therefore, a good fit to the Langmuir model indicates that the adsorption behavior of BLG proteins onto the active sites onto SBA-15-based adsorbents follows the homogeneous and monolayer coverage on the adsorbent surface. In addition, the close proximity between the

calculated adsorption capacities ($Q_{calc.}$) and the experimental ($Q_{max.}$) values further affirms the suitability of this model for interpreting the adsorption processes.

One important parameter is the separation factor (R_L) deduced from the Langmuir isotherm model. R_L is used to identify the feasibility and favorability of the adsorption process and can be obtained using **Eq. (11)**[42]:

$$R_L = \frac{1}{1+bC_{ref}} \quad \textbf{(11)}$$

The value of R_L indicates four types of adsorption behavior: (R_L= 0) unfavorable, (R_L= 1), linear irreversible (R_L> 1), and (0 <R_L<1) favorable[42]. In the context of the adsorption of BLG proteins onto the SBA-15-based adsorbents, the characteristic values determined from the model are reported in **Table S5**. In this study, the values of separation factor (R_L) are found in the range of 0-1, indicating the favorable uptake of the corresponding proteins. Additionally, the values of the Freundlich isotherm constant (K_F) for SBA-15 adsorbents range from 1 to 10, further confirming the feasibility of the adsorption process.

Adsorption thermodynamics

The thermodynamic parameters were also evaluated to better describe the mechanism of BLG adsorption between 278 K and 308 K. The thermodynamic parameters were calculated using **Eqs. (12) (13)**, and **(14)**[43-44]:

$$\Delta G° = \Delta H° - T\Delta S° = - R \times T \times \ln (K) \quad \textbf{(12)}$$

$$\ln(K) = \frac{\Delta S°}{R} - \frac{\Delta H°}{RT} \quad \textbf{(13)}$$

K is the distribution coefficient for adsorption of BLG and is determined as[44]:

$$K = \frac{\boldsymbol{Q_e}}{\boldsymbol{C_e}} \quad \textbf{(14)}$$

where Q_e (g.g^{-1}) is the adsorption capacity at equilibrium, C_e (mg.L^{-1}) is the concentration of BLG at equilibrium, R is the universal gas constant (8.314 J.mol^{-1}.K^{-1}), T is the absolute temperature, ΔG° (kJ.mol^{-1}) is the Gibbs free energy change during adsorption, ΔS° (kJ.mol^{-1}.K^{-1}) and ΔH° (kJ.mol^{-1}) are entropy and enthalpy change, respectively. The values of ΔS° and ΔH° were obtained from the slopes and the intercepts of the linear Van't Hoff plot, *i.e* ln(K) versus 1/T. The thermodynamic parameters are listed in **Table 1**.

The negative values of ΔG° were calculated at temperatures ranging from 278 K to 308 K confirming the feasibility of the process and the spontaneous nature of the adsorption of BLG onto SBA-15-based materials. In addition, the decrease of the absolute values of ΔG° for the SBA-15-SH-5 and SBA-15-SH-10 (even if smaller) adsorbents as temperature increases indicate the lower attractions between the active sites of adsorbents and BLG proteins. For the SBA-15-OH-5 and SBA-15-OH-10 adsorbents, the absolute values of ΔG° increased with increasing temperature, signifying stronger attraction between the active sites of adsorbents and BLG proteins. Generally, for chemical adsorption the values of ΔG° are in the range of -80 to -400 kJ.mol^{-1} and for physical adsorption it ranges between 0 and -20 kJ.mol^{-1} [44]. The values of ΔG° for BLG adsorption onto SBA-15 materials were in the range of -1.48 to -12.54 kJ.mol^{-1}, and thus it is probable that the nature of the adsorption process was predominantly physical adsorption.

Table 1. Thermodynamic parameters for adsorption of BLG proteins onto SBA-15-OH-5, SBA-15-OH-10, SBA-15-SH-5, and SBA-15-SH-10 adsorbents under optimal experimental conditions.

Adsorbent	Temperature (K)	K	ΔG° (kJ.mol^{-1})	ΔS° (J.K^{-1}.mol^{-1})	ΔH° (kJ.mol^{-1})
SBA-15-OH-5	278	1.9	-1.48	97.57	25.64
	288	2.8	-2.49		
	298	4.0	-3.45		
	308	5.6	-4.41		
SBA-15-OH-10	278	41.3	-8.60	69.65	10.76
	288	48.6	-9.30		
	298	56.5	-10.00		
	308	65.1	-10.69		
SBA-15-SH-5	278	24.0	-7.34	-48.33	-20.78
	288	17.6	-6.86		
	298	13.1	-6.38		
	308	10	-5.89		
SBA-15-SH-10	278	249.8	-12.66	-4.08	-13.80
	288	194.9	-12.62		
	298	160.7	-12.58		
	308	134.1	-12.54		

Additionally, the modelled data matched the experimental results obtained from the adsorption isotherms and are supported by the positive value of ΔH° for the SBA-15-OH-5 and SBA-15-OH-10 adsorbents, indicating an endothermic nature of the adsorption process. The positive values of ΔS°, calculated as 97.57 J.mol^{-1}.K^{-1} for SBA-15-OH-5 and 69.65 J.mol^{-1}.K^{-1} for SBA-15-OH-10, are probably related to an increasing disorder and randomness at the adsorbent-solution interface during the adsorption process. This suggests that there is no significant change in the internal mesoporous structure of adsorbent during the adsorption process. In contrast, the negative values of ΔH° for the SBA-15-SH-5 and SBA-15-SH-10 adsorbents, indicate that the adsorption process of BLG proteins onto thiol-functionalized SBA-15 mesoporous adsorbents is exothermic. Additionally, the obtained negative values of ΔS° for

the thiol-functionalized SBA-15 mesoporous adsorbents indicated that there might be a lower affinity between the BLG proteins and the actives sites of the adsorbent surface, possibly due to the disorderliness in the complex formed between thiol groups and BLG proteins or the occurrence of oxidation reactions of thiol groups to sulfonate groups during the adsorption process at higher temperatures. This hypothesis was examined by XPS analysis of the distribution of BLG proteins on the SBA-15-SH-10 adsorbent at 298 K and 308 K (**Fig. 7 (A)** and **(B)**).

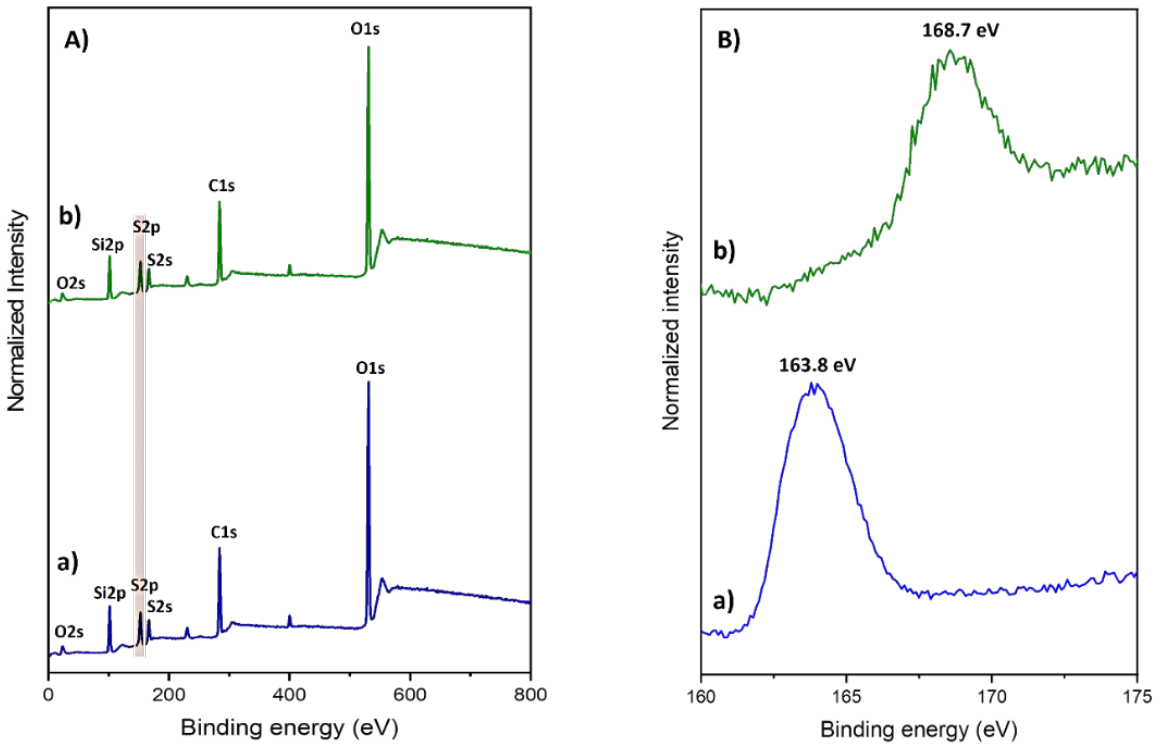

Figure 7. (A) High-resolution X-ray photoelectron spectroscopy spectra for **(a)** SBA-15-SH-10 adsorbent after adsorption of BLG proteins at 298 K and **(b)** SBA-15-SH-10 after adsorption of BLG proteins at 308 K**. (B)** S2p XPS spectra of for **(a)** SBA-15-SH-10+BLG at 298 K and **(b)** SBA-15-SH-10+BLG at 308 K.

Fig. 7 (B) displays the high resolution XPS spectra of S2p for the SBA-15-SH-10 adsorbents after adsorption of BLG proteins at both 298 K and 308 K. In the spectrum obtained at 298 K **(Fig. 7a (B))**, a single band is observed at around 163.8 eV corresponding to S2p, characteristic of sulfur groups (-SH). This confirms the absence of oxidation of the thiol groups to sulfonate groups during the adsorption process of BLG proteins onto SBA-15-SH-10 surface at this temperature. On the other hand, in the spectrum obtained at 308 K **(Fig. 7b (B))**, a strong peak appears at around 168.7 eV due to oxidized thiol groups. This indicates for the SBA-15-SH-10, an oxidation reaction of the thiol groups (-SH) to sulfonate groups ($-SO_3H$), can occur onto the mesoporous material surface at 308 K.

Structural characterizations of SBA-15 materials and BLG by Raman spectroscopy.

To complement these XPS experiments, we used Raman spectroscopy to characterize the mesoporous adsorbent before and after protein absorption at 298 K and 308 K. **Fig. 8** clearly demonstrates that in the functionalized mesoporous, both in the presence and absence of BLG at 308 K, there is an appearance of the SO_3 vibration at 1045 cm^{-1}. Moreover, a shift of the C-S stretching band of the thiol is observed, from 653 cm^{-1} at 298 K to 611 cm^{-1}, in the both mesoporous adsorbents with and without the protein. The presence of SO_3 clearly indicates the occurrence of the oxidation of the S^- group into SO_3^- of the SBA-15-SH-10 material. Additionally, S-S vibration which may appear at 470 cm^{-1} is not observed in the functionalized mesoporous with and without the protein. It is important to emphasize that the amount of adsorbed BLG is low, with values of 1.45 and 2.16 $mmol.g^{-1}$ for SBA-15-SH-5 and SBA-15-SH-10, respectively. Even if S-S interactions occurred, their detection using Raman spectroscopy is challenging due to the limited number of S-S and SH groups (only two S-S and one SH in BLG molecule) and their specific location within the protein structure.

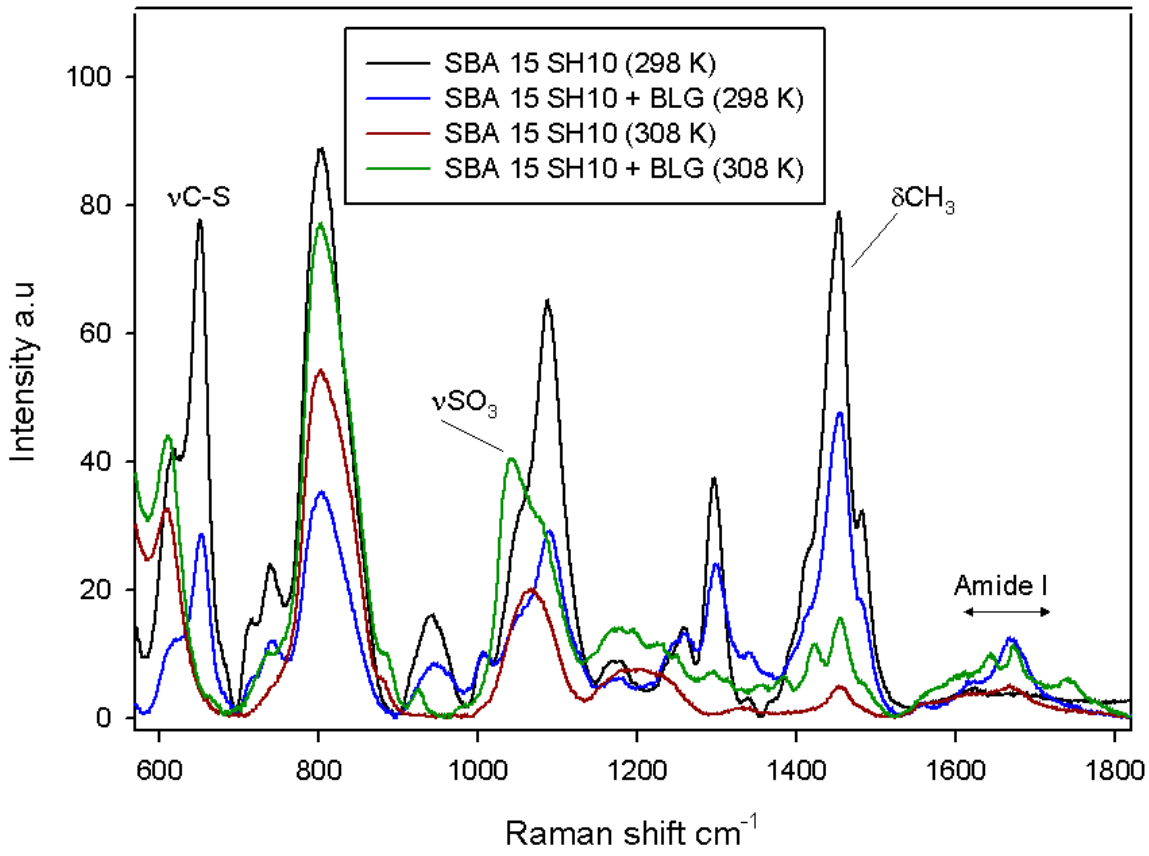

Figure 8. Raman spectroscopy spectra for **(black)** SBA-15-SH-10 adsorbent at 298 K, **(blue)** SBA-15-SH-10 after adsorption of BLG proteins at 298 K and **(green)** SBA-15-SH-10 after adsorption of BLG proteins at 308 K**.**

We have also compared the bands of the adsorbents with different pore sizes (5 and 10 nm) before and after the absorption of BLG at 298 K. The spectra presented in Figure 9 indicate that there is no significant difference of the vibration pattern of the two mesoporous materials. The Amide I band of the proteins absorbed on mesoporous materials with 5 or 10 nm is very similar and shows a secondary protein structure which is composed of β sheets, which is typical for β-lactoglobulin.

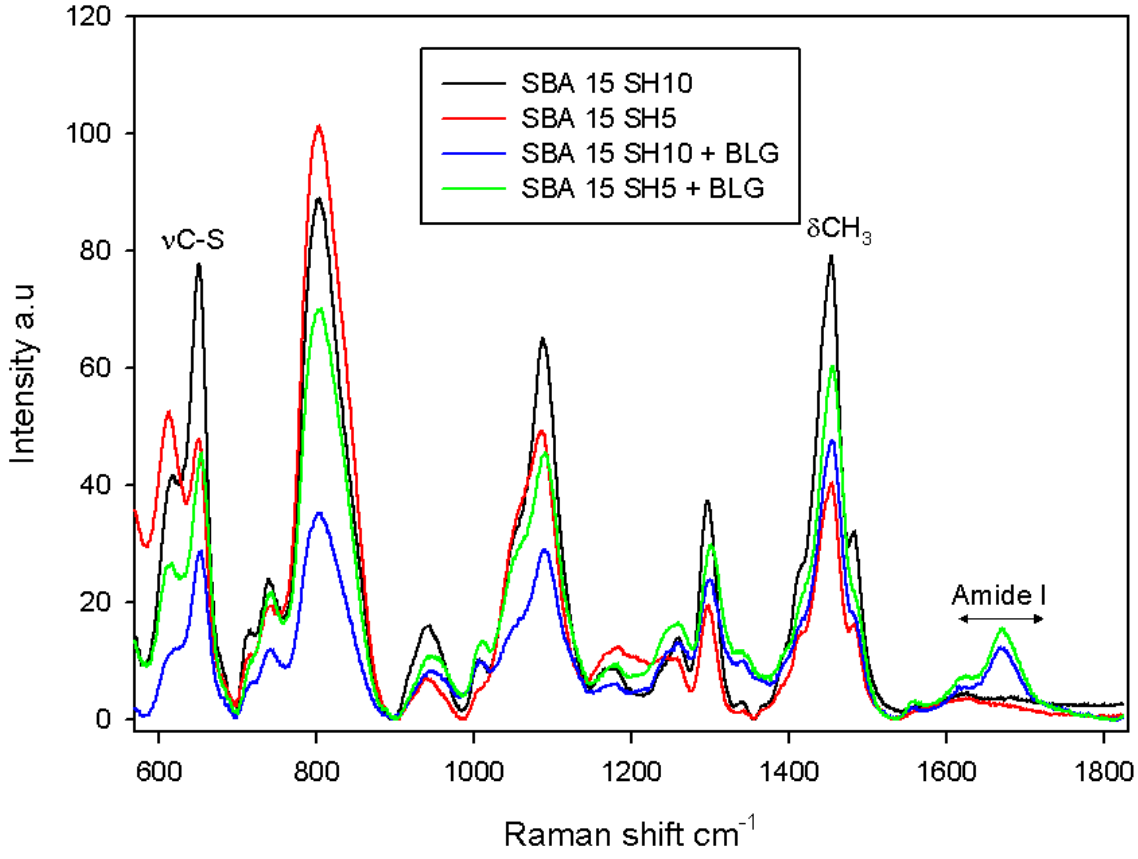

Figure 9. Raman spectroscopy spectra for SBA-15-SH-10 adsorbent at 298 K **(black)**, SBA-15-SH-5 absorbent at 298 K **(red)**, and on the same materials after adsorption of BLG proteins at 298 K, on SBA-15-SH-10 + BLG **(blue),** and SBA-15-SH-5 + BLG **(green).**

So, through these Raman spectroscopy experiments, we have confirmed that oxidation of the thiol groups in the absorbent occurs at 308 K. Both mesoporous materials (5 and 10 nm pores sizes) can adsorb the proteins without major changes to their structure, and the protein itself keeps its structure after adsorption. The oxidation observed at high temperature could increase the affinity of the adsorption of the protein to the mesoporous through electrostatic interactions between SO_3^- and amine groups of BLG. This can be confirmed by the increase in absolute value of the free energy observed at high temperatures (**Table 1**).

Comparison of the adsorption capacities of different adsorbents for β-lactoglobulin (BLG) proteins.

A detailed comparison of the maximum adsorption capacities of SBA-15-OH-5, SBA-15-SH-5, SBA-15-OH-10, and SBA-15-SH-10 adsorbents with various previously used adsorbents for β-lactoglobulin (BLG) proteins is presented in Table S7. For instance, Sarvi et *al.* prepared FDU-12-120-NH_2 with a pore size of 6.1 nm for the adsorption of β-lactoglobulin at pH= 7, achieving a maximum adsorption capacity of 0.143 $g.g^{-1}$ [38]. In contrast, Chen et *al.* synthesized a novel polyoxometalate (POM)-based organic–inorganic hybrid, $[C_{33}H_{24}O_4]H_3PMo_{12}O_{40}$ (TPPA-PMo_{12}), *via* a one-pot hydrothermal reaction[45]. This hybrid showed excellent adsorption performance for β-lactoglobulin, with a 99.2 % adsorption efficiency at pH 5.0 using 0.5 mg of TPPA-PMo_{12} for 100 $mg.mL^{-1}$ of β-lactoglobulin in 1.0 mL solution. The adsorption behavior of β-lactoglobulin followed the Langmuir model, with a theoretical adsorption capacity of 1.428 $g.g^{-1}$. **Table S7** highlights that the pore sizes and thiol groups of SBA-15-based adsorbents significantly influence BLG adsorption capacities. Notably, the thiol-functionalized SBA-15 with a 10 nm pore size (SBA-15-SH-10) exhibited the highest adsorption capacity of 0.560 $g.g^{-1}$ under optimal conditions, which is approximately five times higher than that of the FDU-12-120-NH_2 adsorbent. From this table we can clearly see that the functionalization with thiol is an adding value for the reactivity of the mesoporous material. Indeed, without thiol or amine groups, the material presents very low adsorption capacity (0.034 $g.g^{-1}$ for SBA-15-OH-5).

This behavior can be attributed to the higher affinity of β-lactoglobulin (BLG) proteins for the heterogeneous active adsorption sites on functionalized materials. This affinity arises from the interactions between the BLG proteins, moreover the disulfide bridges of the proteins (Cys66-Cys160 and Cys106-Cys119) and the thiol groups on SBA-15-based materials. Additionally, the porous structure of the SBA-15-based materials facilitates the diffusion of BLG proteins into the adsorbent pores, thereby increasing the overall adsorption capacity. The

interplay of these molecular interactions and the structural compatibility between the BLG proteins and the SBA-15-based materials underscores the effectiveness of this adsorption process. An illustrative scheme of the cooperative adsorption mechanism between BLG protein and the different mesoporous materials is proposed in Figure 10. Such findings align with studies indicating that adsorbents' surface chemistry and pore architecture significantly influence protein adsorption behavior, particularly for proteins with complex structures like BLG[38,45]. Another parameter which can improve the reactivity of the functionalized mesoporous material is the pH, as at higher pH, the reactivity of the thiol can be higher with 100% of the the thiol on the deprotonated form (pKa of the thiol 8.4). However, at pH values superior to the pKa of the thiol, pH > 8.4, the stability of the protein can be lower.

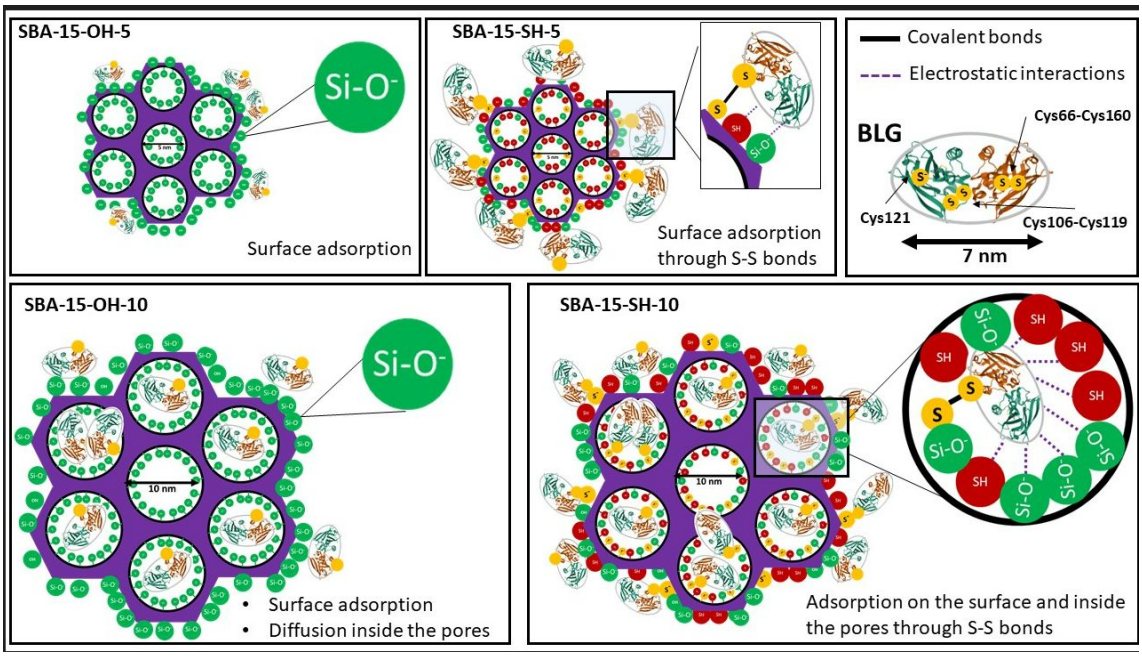

Figure 10. Illustrative scheme of the cooperative adsorption mechanism between a BLG protein and the active adsorption sites onto SBA-15-OH-10, SBA-15-OH-5, SBA-15-SH-10 and SBA-15-SH-5 adsorbents.

CONCLUSION

This study systematically investigated the synthesis and application of thiol-functionalized SBA-15 materials with varying pore sizes to enhance the adsorption behavior of mesoporous SBA-15 towards β-lactoglobulin (BLG) proteins. The findings provide critical insights into the interplay between pore characteristics, surface functionalization, and protein adsorption behavior. Among tested adsorbents, SBA-15-SH-10 showed the highest adsorption capacity (0.560 ± 0.01 $g.g^{-1}$) under optimal experimental conditions ([BLG]= 9 $g.L^{-1}$, pH= 7, and T= 298 K). The observed superior adsorption capacity of SBA-15-SH-10 compared to other tested adsorbents underscores the importance of optimizing both pore size and thiol-silane grafting density on the silica surface. The enhanced adsorption capacity of SBA-15-SH-10 can be attributed to a combination of factors, including increased surface area, pore volume, and accessible surface functional groups conducive to protein binding. The kinetics of BLG protein adsorption onto SBA-15-SH-10 followed pseudo-second order (PSO) and Bangham's models, suggesting a complex adsorption mechanism characterized by multilayer adsorption within the pores with heterogeneous surfaces. This behavior highlights the significance of mesoporous structure in facilitating efficient protein adsorption, with the presence of thiol functional groups further enhancing binding interactions. The Langmuir model provided the best fit for the adsorption isotherm studies, indicating monolayer adsorption behavior and suggesting the formation of a homogeneous protein layer on the adsorbent surface. This monolayer formation is facilitated by specific interactions between BLG proteins and thiol-functionalized surface sites, leading to enhanced adsorption capacity and selectivity. Thermodynamic analysis revealed that the adsorption process onto SBA-15-SH-5 and SBA-15-SH-10 adsorbents is exothermic and spontaneous, driven by favorable interactions between BLG proteins and the adsorbent surface. The decrease in surface entropy upon thiol group oxidation to sulfonate

groups at 308 K indicates a reduction in surface randomness, further corroborating the specificity of protein adsorption onto functionalized surfaces. In contrast, the endothermic nature of adsorption onto non-functionalized SBA-15 mesoporous adsorbents suggests weaker interactions and lower adsorption capacities, emphasizing the crucial role of surface functionalization in enhancing protein binding affinity. Raman spectroscopy provided additional evidence of thiol group oxidation at 308 K, confirming the chemical transformation of surface functional groups during the adsorption process. Importantly, the negligible impact of protein adsorption on the secondary structure of BLG proteins suggests minimal structural perturbation, highlighting the biocompatibility and preservation of protein integrity during the adsorption process. In perspectives of this work, it will be interesting to study the release of the proteins adsorbed on the SBA-15-SH-5 and SH-10 materials by addition of dithiothreitol for example. A study as function of the pH can also bring a better understanding of the mechanism of interaction of the proteins with the different mesoporous materials. Lower pH (lower than the pHi of the BLG, so lower that 5.2) should higher the adsorption of the protein on the SBA-15- OH materials through electrostatic interaction. At higher pH value (higher than the pKa of the thiol, so pH > 8.4), the majority of the thiol of the functionalized mesoporous materials will be on their deprotonated S^- form and so more reactive. Finally, one can also functionalized the proteins by succinylation, or increase the accessibility of the disulfide bridge of the BLG by its partial unfolding. The results of the present study and those of these perspectives will guide the development of scalable, cost-effective adsorbents for practical applications in drug delivery and biotechnology, aligning with green chemistry principles and enhancing economic viability.

ASSOCIATED CONTENT

Supporting Information

Structural characteristics, Small-angle XRD patterns, Transmission electron microscopy (TEM) images, FTIR spectra, XPS Survey scan, TGA analyses, Kinetic parameters calculated, and Values of the isotherm parameters calculated, Comparison of the adsorption capacities of various adsorbents for BLG proteins from aqueous solutions.

Corresponding Authors

Laroussi Chaabane- *Université Bourgogne Franche-Comté, Institut Agro, Université Bourgogne, INRAE, UMR PAM 1517, 21000 Dijon, France*.

Email: laroussichaabane92@gmail.com

Camille Loupiac- *Université Bourgogne Franche-Comté, Institut Agro, Université Bourgogne, INRAE, UMR PAM 1517, 21000 Dijon, France*

Email: camille.loupiac@agrosupdijon.fr

Authors

Laroussi Chaabane-*Université Bourgogne Franche-Comté, Institut Agro, Université Bourgogne, INRAE, UMR PAM 1517, 21000 Dijon, France*

Camille Loupiac-*Université Bourgogne Franche-Comté, Institut Agro, Université Bourgogne, INRAE, UMR PAM 1517, 21000 Dijon, France*

Frédéric Bouyer-Laboratoire Interdisciplinaire Carnot de Bourgogne, CNRS-Université de Bourgogne, 9 Avenue Alain Savary, BP 47 870, 21078 Dijon Cedex, France.

Igor Bezverkhyyb-Laboratoire Interdisciplinaire Carnot de Bourgogne, CNRS-Université de Bourgogne, 9 Avenue Alain Savary, BP 47 870, 21078 Dijon Cedex, France.

Sarah Foley-Laboratoire Chrono-environnement (UMR CNRS 6249), Univ. Bourgogne Franche Comté, F-25000 Besançon, France.

Ali Assifaoui-Department of pharmaceutical Technology, School of Pharmacy, Université de Bourgogne, 7 Bd Jeanne d'Arc, 21079 Dijon, France.

Notes

The authors declare that they have no known competing financial interests or personal relationships that could have appeared to influence the work reported in this paper.

ACKNOWLEDGMENT

The authors gratefully acknowledge the financial support from **Institut Agro Sup Dijon-France** for Postdoc position-2022 and **Valvigne project** (SYNERGIE BG0027582). We acknowledge Dr N. Geoffroy, R. Chassagnon and Dr A. Kristiania for their advice in XRD, TEM, and XPS characterization, respectively. Mrs B. Rollin (UMR PAM, team PCAV) is also acknowledged for the purification of the β-lactoglobulin and technical support in the biochemistry laboratory of the PCAV team. We acknowledge the DIVVA platform (AgroSup Dijon, Université Bourgogne Franche Comté) for the various physicochemical characterizations.

REFERENCE

(1) Danesh-khorasgani, M.; Faghihian, H.; Givianrad, M. H.; Aberoomand-Azar, P.; & Saber-Tehrani, M. Synthesis and application of a novel mesoporous SBA-15 sorbent functionalized by 2, 4 dinitrophenylhydrazine (DNPH) for simultaneous removal of Pb (II), Cr (III), Cd (II) and Co (II) from aqueous solutions: Experimental design, kinetic, thermodynamic, and isotherm aspects. Advanced Powder Technology, 2022, 33, 103201.

(2) Varache, M.; Bezverkhyy, I.; Weber, G.; Saviot, L.; Chassagnon, R.; Baras, F.; Bouyer F. Loading of cisplatin into mesoporous silica nanoparticles: Effect of surface functionalization, Langmuir, **2019**, 35, 8984-8995.

(3) Appaturi, J. N.; Pulingam, T.; Rajabathar, J. R.; Khoerunnisa, F.; Ling, T. C.; Tan, S. H.; Ng, E. P. Acid-base bifunctional SBA-15 as an active and selective catalyst for synthesis of ethyl α-cyanocinnamate via Knoevenagel condensation, Microporous and Mesoporous Materials, **2021**, 320, 111091.

(4) Diaz, J. F.; Balkus Jr, K. J. Enzyme immobilization in MCM-41 molecular sieve, Journal of Molecular Catalysis B: Enzymatic **1996**, 2(2-3), 115-126.

(5) Falahati, M.; Saboury, A. A.; Shafiee, A.; Sorkhabadi, S. M. R.; Kachooei, E.; Ma'Mani, L.; Haertlé, T. Highly efficient immobilization of beta-lactoglobulin in functionalized mesoporous nanoparticles: A simple and useful approach for enhancement of protein stability, Biophysical Chemistry, **2012**, 165, 13-20.

(6) Zhou, Z.; Hartmann, M. Progress in enzyme immobilization in ordered mesoporous materials and related applications, Chemical Society Reviews, **2013**, 42(9), 3894-3912.

(7) Carlsson, N.; Gustafsson, H.; Thörn, C.; Olsson, L.; Holmberg, K.; Åkerman, B. Enzymes immobilized in mesoporous silica: A physical–chemical perspective. Advances in colloid and interface science, **2014**, 205, 339-360.

(8) Costantini, A.; Califano, V. Lipase immobilization in mesoporous silica nanoparticles for biofuel production, Catalysts, **2021**, 11(5), 629.

(9) Salis, A.; Medda, L.; Cugia, F.; Monduzzi, M. Effect of electrolytes on proteins physisorption on ordered mesoporous silica materials. Colloids and Surfaces B: Biointerfaces, **2016**, 137, 77-90.

(10) Lashgari, N.; Badiei, A.; Ziarani, G. M. A novel functionalized nanoporous SBA-15 as a selective fluorescent sensor for the detection of multianalytes (Fe3+ and Cr2O72−) in water. Journal of Physics and Chemistry of Solids, **2017**, 103 238-248.

(11) Costa, J. A. S.; de Jesus, R. A.; Santos, D. O.; Neris, J. B.; Figueiredo, R. T.; Paranhos, C. M. Synthesis, functionalization, and environmental application of silica-based mesoporous materials of the M41S and SBA-n families: A review. Journal of Environmental Chemical Engineering, **2021**, 9, 105259.

(12) Chaudhuri, H.; Dash, S.; Sarkar, A. SBA-15 functionalised with high loading of amino or carboxylate groups as selective adsorbent for enhanced removal of toxic dyes from aqueous solution. New Journal of Chemistry, **2016**, 40, 3622-3634.

(13) Dash, S.; Chaudhuri, H.; Gupta, R.; Nair, U. G.; Adsorption study of modified coal fly ash with sulfonic acid as a potential adsorbent for the removal of toxic reactive dyes from aqueous solution: Kinetics and thermodynamics. Journal of Environmental Chemical Engineering, **2018**, 6, 5897-5905.

(14) Vavsari, V. F.; Ziarani, G. M.; Badiei, A.; The role of SBA-15 in drug delivery.RSC Advances, **2015**, 5, 91686-91707.

(15) Hassanzadeh-Afruzi, F.; Asgharnasl, S.; Mehraeen, S.; Amiri-Khamakani, Z.; Maleki, A.; Guanidinylated SBA-15/Fe3O4 mesoporous nanocomposite as an efficient catalyst for the synthesis of pyranopyrazole derivatives. Scientific Reports, **2021,** 11, 19852.

(16) Do Valle Gomes, M. Z.; Zadeh, P. S. N.; Palmqvist, A. E.; Åkerman, B. Spatial Distribution of Enzymes Immobilized in Mesoporous Silicas for Biocatalysis. ACS Appl Nano Mater, **2019**, 2, 7245-7254.

(17) Miao, H.; Li, M.; Wang, F.; Li, J.; Lin, Y. W.; Xu, J. Surface Functionalization of SBA-15 for Immobilization of Myoglobin. Frontiers in Bioengineering and Biotechnology, **2022**, 10, 907855.

(18) Kontopidis, G.; Holt, C.; Sawyer, L. Invited review: β-lactoglobulin: binding properties, structure, and function. Journal of dairy science, **2004**, 87(4), 785-796.

(19) Stanić-Vučinić, D.; Ćirković-Veličković, T. The modifications of bovine beta-lactoglobulin-effects on its structural and functional properties. Journal of the Serbian Chemical Society, **2013**, 78(3), 445-461.

(20) Maire du Poset, A.; Börjesson, M. ; Rameau, C.; Madeleine-Perdrillat, C.; Lerbret, A.; Loupiac, C.; Assifaoui, A. Controlled loading and release of beta-lactoglobulin in calcium-polygalacturonate hydrogels.Biomacromolecules, **2020**, 21(4), 1417-1426.

(21) Sakai, K.; Sakurai, K.; Sakai, M.; Hoshino, M.; Goto, Y.; Conformation and stability of thiol-modified bovine β lactoglobulin. Protein Science, **2000**, 9(9), 1719-1729.

(22) Kinsella, J. E.; Whitehead, D. M. Proteins in whey: chemical, physical, and functional properties. Advances in food and nutrition research, **1989**, 33, 343-438.

(23) Bunsroem, K.; Prinyawiwatkul, W.; Thaiudom, S. The influence of whey protein heating parameters on their susceptibility to digestive enzymes and the antidiabetic activity of hydrolysates. Foods, **2022**, 11(6), 829.

(24) Brownlow S.; Cabral J.H.M.; Cooper R.; Flower D.R.; Yewdall S.J.; Polikarpov I.; North A.C.T.; Sawyer L. Bovine β-lactoglobulin at 1.8 Å resolution—still an enigmatic lipocalin. Structure, **1997**, 5, 481-495.

(25) Fox, K. K.; Holsinger, V. H.; Pallansch. M. H.; J. Separation of β-lactoglobulin from other milk serum proteins by trichloroacetic acid. Journal of Dairy Science, **1967**, 50, 1363–1367.

(26) Zhao, D. Y.; Huo, Q. S.; Feng, J. L.; Chmelka, B. F.; Stucky, G. D. Nonionic triblock and star diblock copolymer and oligomeric surfactant syntheses of highly ordered, hydrothermally stable, mesoporous silica structures. J. Am. Chem. Soc. **1998**, 120 (24), 6024−6036.

(27) Gustafsson, H.; Thorn, C.; Holmberg, K. A comparison of lipase and trypsin encapsulated in mesoporous materials with varying pore sizes and pH conditions, Colloids Surf., B, **2011**, 87 (2), 464−471.

(28) Hafezian, S. M.; Biparva, P.; Bekhradnia, A.; Azizi, S. N.; Amine and thiol functionalization of SBA-15 nanoparticles for highly efficient adsorption of sulforaphane, Advanced Powder Technology, **2021**, 32 779-790.

(29) Miao, H.; Li, M.; Wang, F.; Li, J.; Lin, Y. W.; Xu, J. Effects of pore size and crosslinking methods on the immobilization of myoglobin in SBA-15. Frontiers in Bioengineering and Biotechnology, **2022**, 9, 827552.

(30) Chaabane, L.; Nikolantonaki, M.; Weber, G.; Bezverkhyy, I.; Chassagnon, R.; Assifaoui, A., Bouyer, F. Functionalization of SBA-15 mesoporous silica for highly efficient adsorption of glutathione: Characterization and modeling studies. Journal of the Taiwan Institute of Chemical Engineers, **2023**, 152, 105169.

(31) Bazzaz, F.; Binaeian E.; Heydarinasan, A.; Ghadi, A. Adsorption of BSA onto hexagonal mesoporous silicate loaded by APTES and tannin: Isotherm, thermodynamic and kinetic studies. Advanced Powder Technology, **2018**, 29(7), 1664-1675.

(32) Wu, Y.–; Qi, H.; Li, B.; Zhanhua, H.; Li, W.; Liu, S. Novel hydrophobic cotton fibers adsorbent for the removal of nitrobenzene in aqueous solution. Carbohydrate Polymers, **2017**, 155, 294-302.

(33) Chaabane, L.; Beyou, E.; Luneau, D.; Baouab, M. H. V. Functionalization of graphene oxide sheets with magnetite nanoparticles for the adsorption of copper ions and investigation of its potential catalytic activity toward the homocoupling of alkynes under green conditions. Journal of catalysis, **2020**, 388, 91-103.

(34) Aharoni, C.; Sideman, S.; Hoffer, E. Adsorption of phosphate ions by collodion-coated alumina. Journal of Chemical Technology and Biotechnology, **1979**, 29(7), 404-412.

(35) Kavitha, D.; Namasivayam, C. Experimental and kinetic studies on methylene blue adsorption by coir pith carbon. Bioresource technology, **2007**, 98(1), 14-21.

(36) Shen, Y.; Jiang, N.; Liu, S.; Zheng, C.; Wang, X.; Huang, T.; Bai, R. Thiol functionalization of short channel SBA-15 through a safe, mild and facile method and application for the removal of mercury (II). Journal of environmental chemical engineering, **2018**, 6(4), 5420-5433.

(37) Mercadante, D.; Melton, L. D.; Norris, G. E.; Loo, T. S.; Williams, M. A.; Dobson, R. C.; Jameson, G. B. Bovine β-lactoglobulin is dimeric under imitative physiological conditions: dissociation equilibrium and rate constants over the pH range of 2.5–7.5. Biophysical Journal, **2012,**103(2), 303-312.

(38) Sarvi, M. N.; Bee, T. B.; Gooi, C. K.; Woonton, B. W.; Gee, M. L.; O'Connor, A. J. Development of functionalized mesoporous silica for adsorption and separation of dairy proteins. Chemical Engineering Journal, **2014**, 235, 244-251.

(39) Majd, M. M.; Kordzadeh-Kermani, V.; Ghalandari, V.; Askari, A.; Sillanpää, M. Adsorption isotherm models: A comprehensive and systematic review (2010−2020). Science of The Total Environment, **2021**, 151334.

(40) Langmuir, I.; The constitution and fundamental properties of solids and liquids. Journal of the American chemical society, **1916**, 38(11), 2221-2295.

(41) Chaabane, L.; Beyou, E.; El Ghali, A.; Baouab, M. H. V. Comparative studies on the adsorption of metal ions from aqueous solutions using various functionalized graphene oxide sheets as supported adsorbents. Journal of hazardous materials, **2020**, 389, 121839.

(42) Chaabane, L.; Beyou, E.; Baouab, M. H. V. Preparation of a novel zwitterionic graphene oxide-based adsorbent to remove of heavy metal ions from water: Modeling and comparative studies. Advanced Powder Technology, **2021**, 32(7), 2502-2516.

(43) Fil, B. A.; Korkmaz, M.; Ozmetin, G, An empirical model for adsorption thermodynamics of copper (II) from solutions onto illite clay-batch process design. Journal of the Chilean Chemical Society, **2014**, 59(4), 2686-2691.

(44) Juengchareonpoon, K.; Wanichpongpan, P.; Boonamnuayvitaya, V. Graphene oxide and carboxymethylcellulose film modified by citric acid for antibiotic removal. Journal of Environmental Chemical Engineering, **2021**, 9(1), 104637

(45) Chen, Q.; Zhang, D. D.; Wang, M. M.; Chen, X. W.; Wang, J. H. A novel organic–inorganic hybrid polyoxometalate for the selective adsorption/isolation of β-lactoglobulin. Journal of materials chemistry B, **2015**, 3(34), 6964-6970.

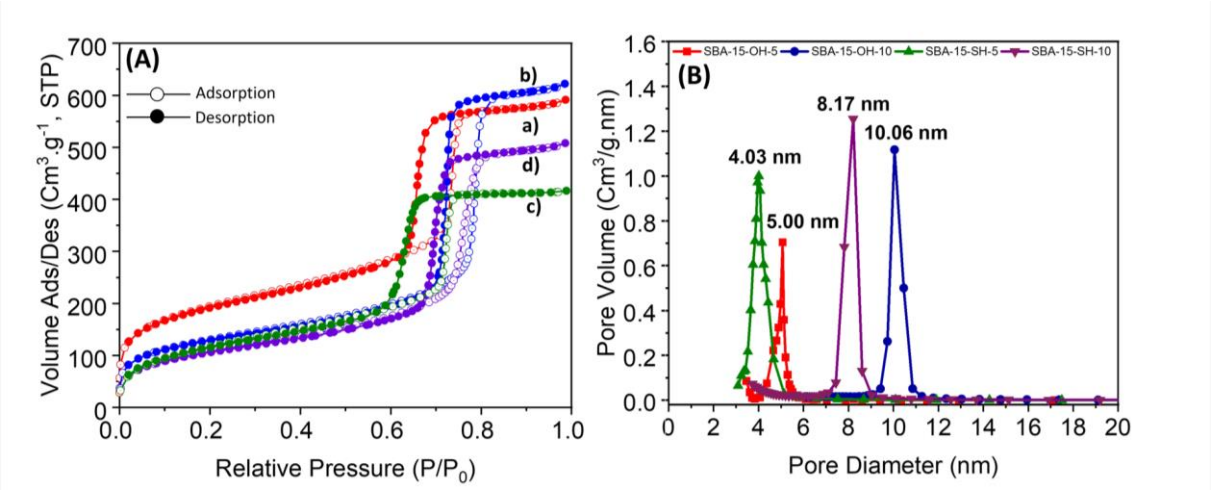
(A)
Adsorption
Desorption
b)
a)
d)
c)
Volume Ads/Des (Cm3.g-1, STP)
Relative Pressure (P/P0)
(B)
SBA-15-OH-5
SBA-15-OH-10
SBA-15-SH-5
SBA-15-SH-10
4.03 nm
5.00 nm
8.17 nm
10.06 nm
Pore Volume (Cm3/g.nm)
Pore Diameter (nm)

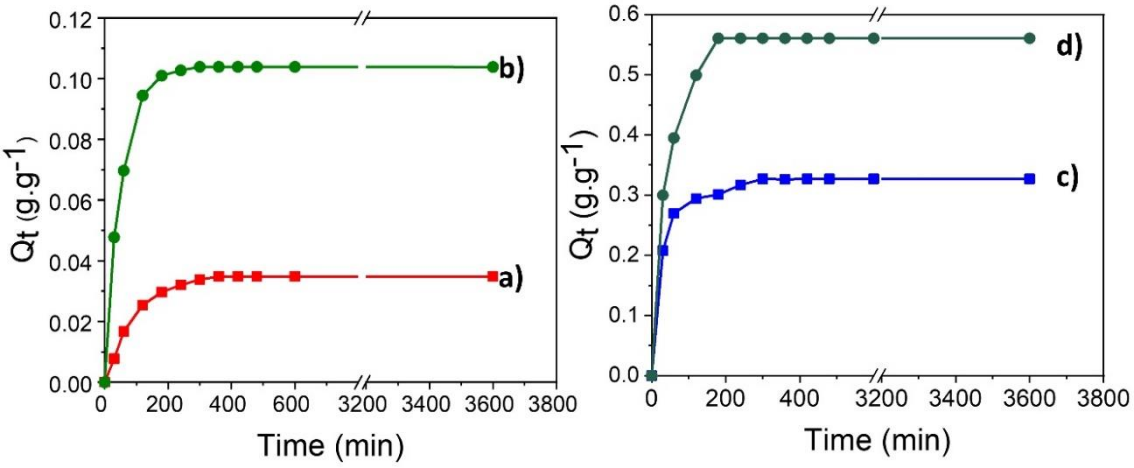
Qt (g.g-1)
Time (min)
b)
a)
d)
c)

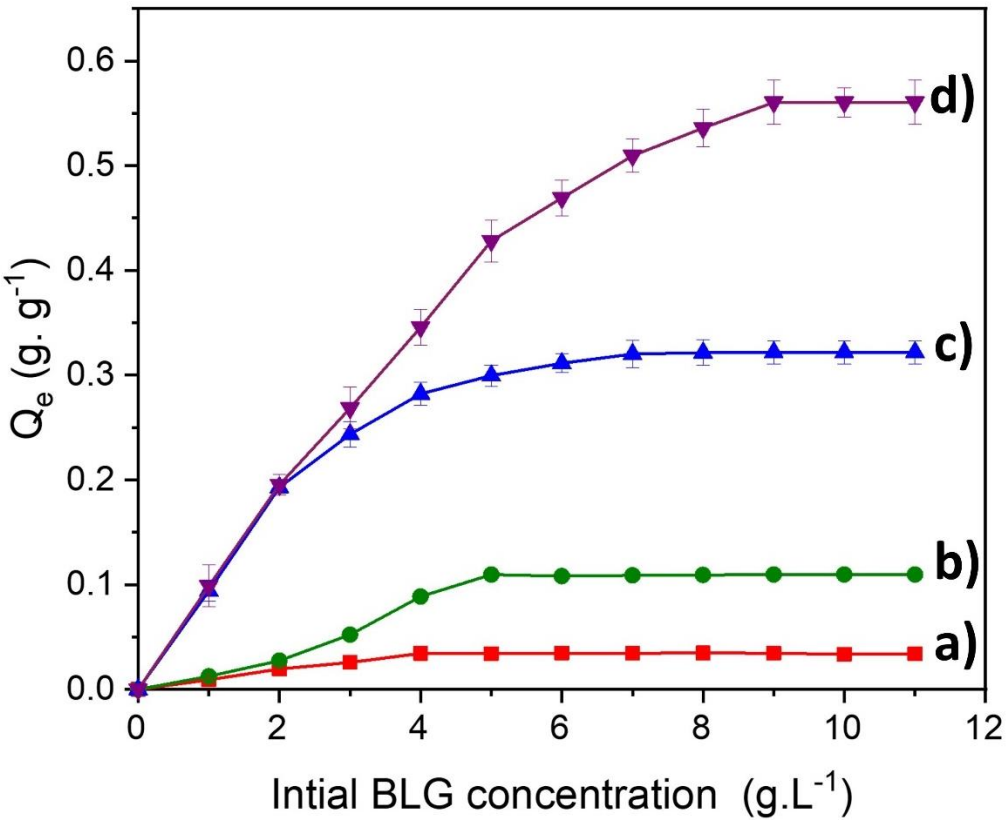
0.6
0.5
0.4
0.3
0.2
0.1
0.0
Q_e (g. g^{-1})
0
2
4
6
8
10
12
Intial BLG concentration (g.L^{-1})
d)
c)
b)
a)

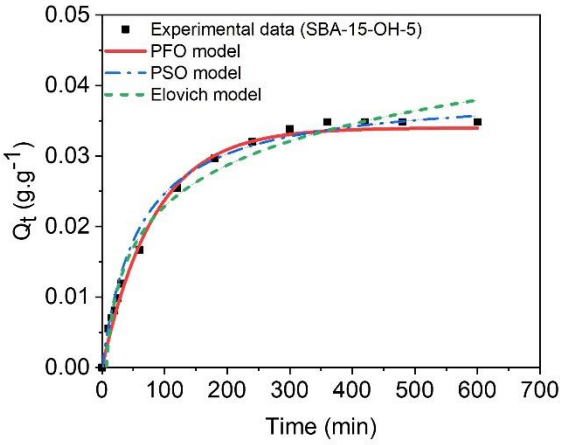
Experimental data (SBA-15-OH-5)
PFO model
PSO model
Elovich model
Q_t (g.g^{-1})
Time (min)

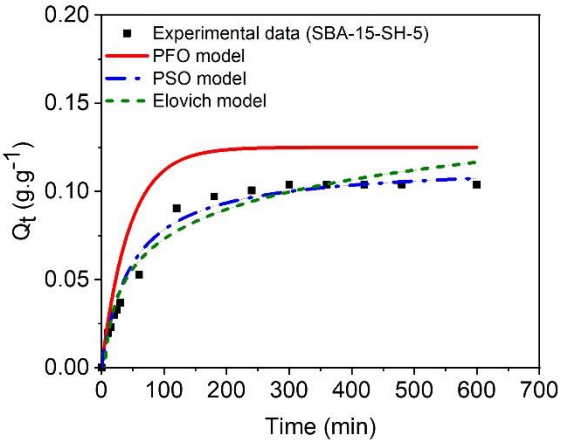
Experimental data (SBA-15-SH-5)
PFO model
PSO model
Elovich model
Q_t (g.g^{-1})
Time (min)

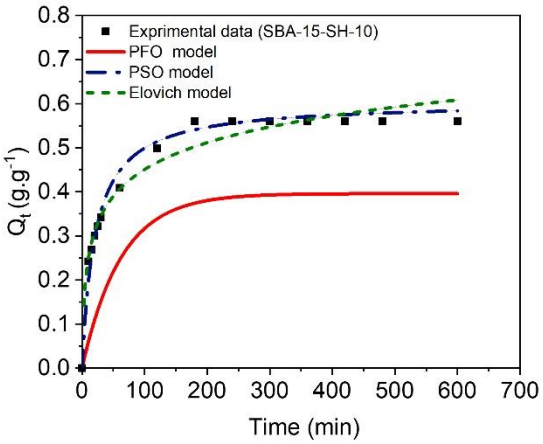
Exprimental data (SBA-15-SH-10)
PFO model
PSO model
Elovich model
Q_t (g.g^{-1})
Time (min)

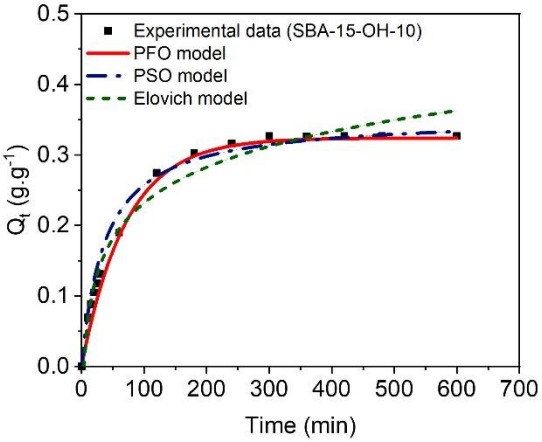
Experimental data (SBA-15-OH-10)
PFO model
PSO model
Elovich model
Q_t (g.g^{-1})
Time (min)

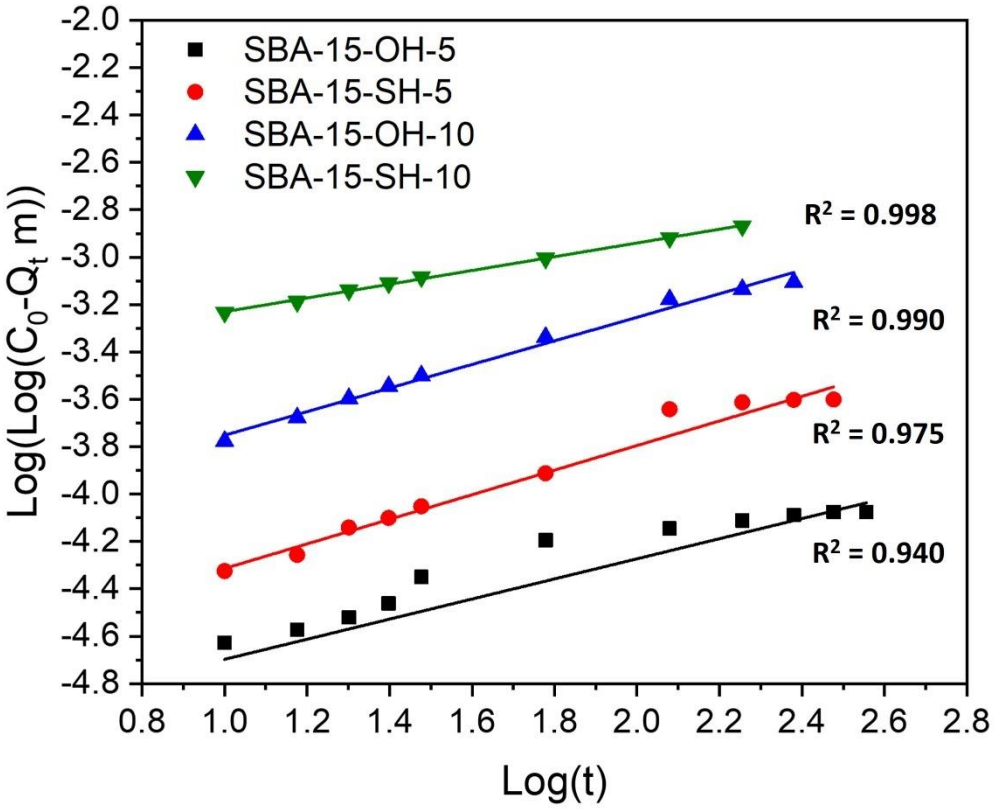
SBA-15-OH-5
SBA-15-SH-5
SBA-15-OH-10
SBA-15-SH-10
R² = 0.998
R² = 0.990
R² = 0.975
R² = 0.940
Log(Log(C0-Qt m))
Log(t)
-2.0
-2.2
-2.4
-2.6
-2.8
-3.0
-3.2
-3.4
-3.6
-3.8
-4.0
-4.2
-4.4
-4.6
-4.8
0.8
1.0
1.2
1.4
1.6
1.8
2.0
2.2
2.4
2.6
2.8

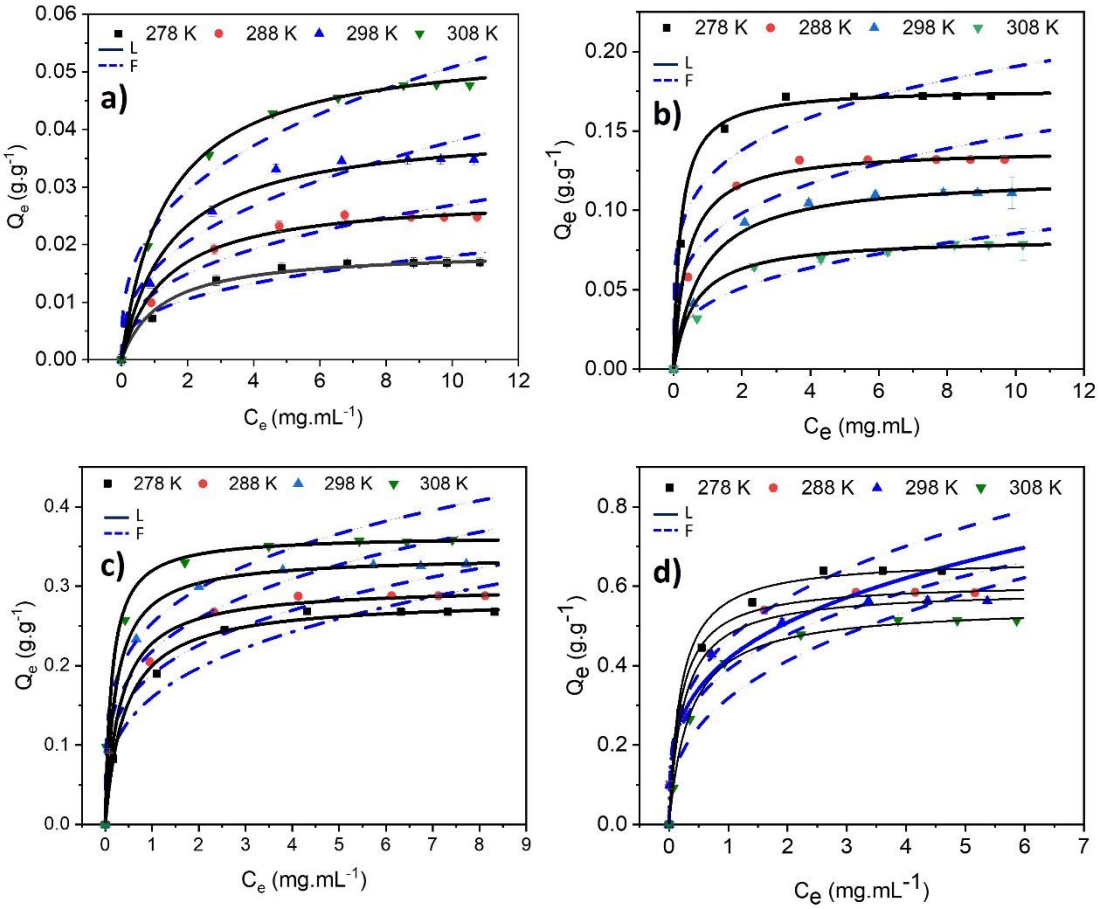
278 K
288 K
298 K
308 K
L
F
a)
b)
c)
d)
Q_e (g.g^{-1})
C_e (mg.mL^{-1})
C_e (mg.mL)

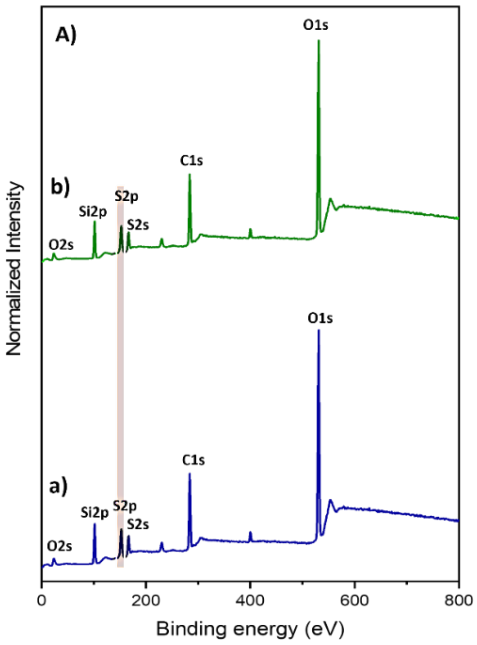
A)
O1s
C1s
b)
Si2p
S2p
S2s
O2s
O1s
C1s
a)
Si2p
S2p
S2s
O2s
Normalized Intensity
0
200
400
600
800
Binding energy (eV)

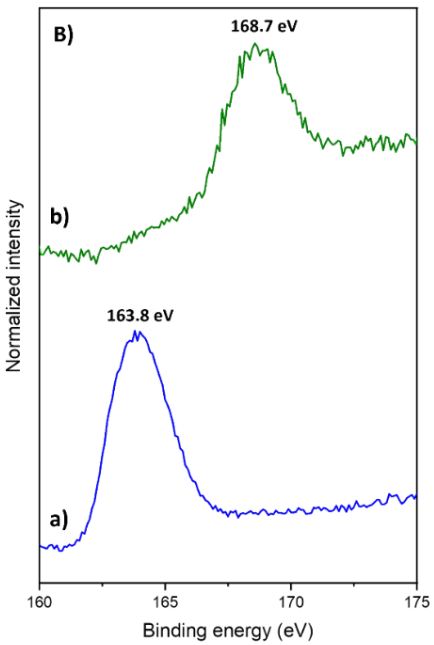
B)
168.7 eV
b)
163.8 eV
a)
Normalized intensity
160
165
170
175
Binding energy (eV)

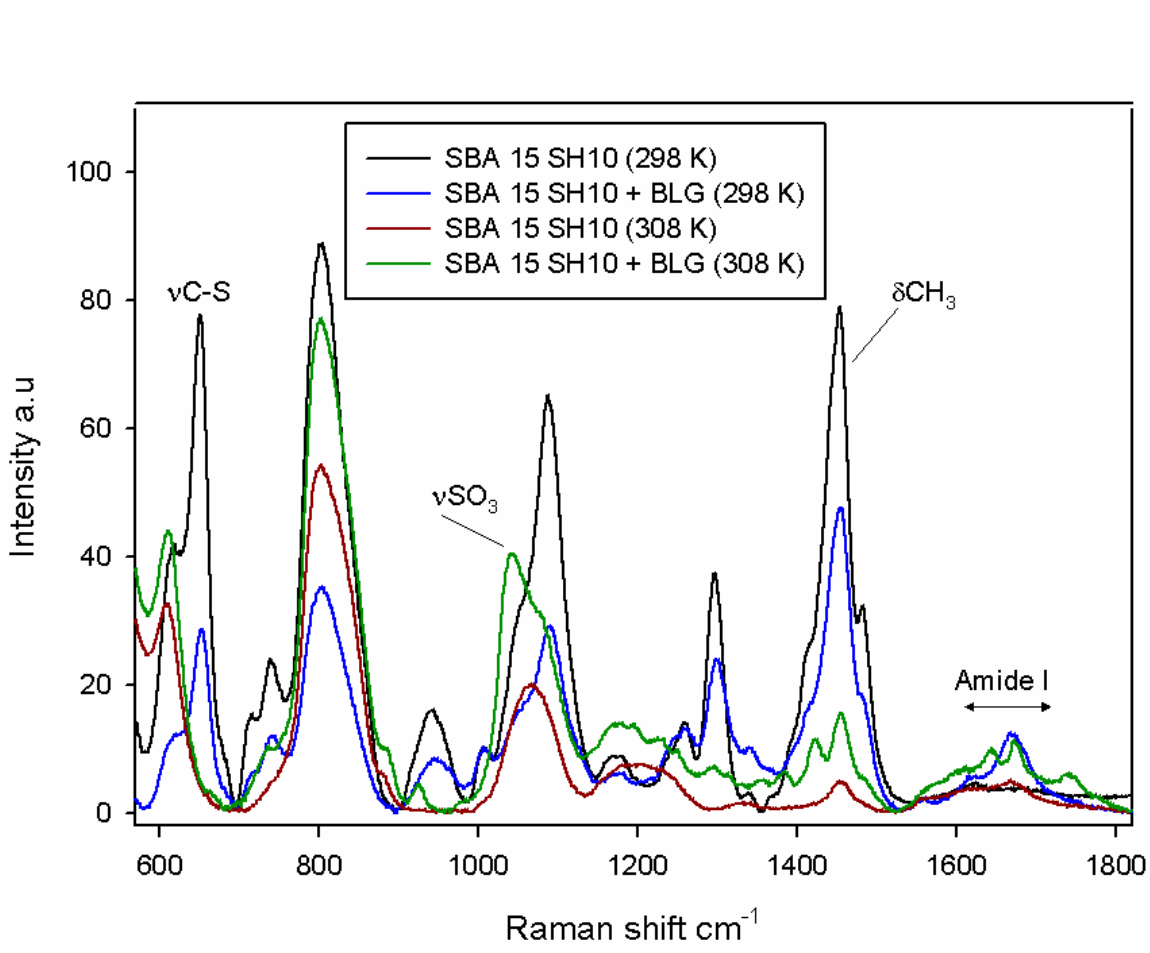
SBA 15 SH10 (298 K)
SBA 15 SH10 + BLG (298 K)
SBA 15 SH10 (308 K)
SBA 15 SH10 + BLG (308 K)
νC-S
νSO3
δCH3
Amide I
Intensity a.u
Raman shift cm-1
0
20
40
60
80
100
600
800
1000
1200
1400
1600
1800

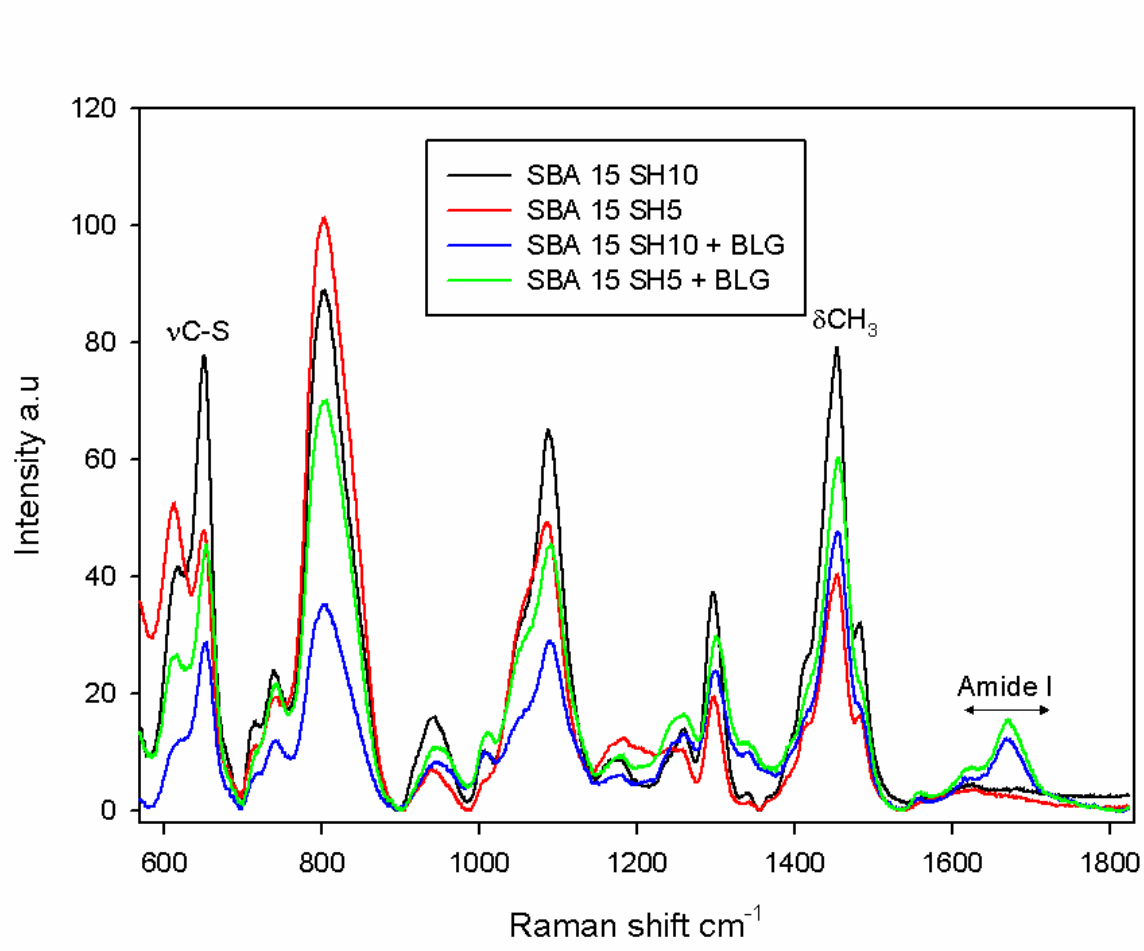
SBA 15 SH10
SBA 15 SH5
SBA 15 SH10 + BLG
SBA 15 SH5 + BLG
νC-S
δCH3
Amide I
Intensity a.u
Raman shift cm-1
0
20
40
60
80
100
120
600
800
1000
1200
1400
1600
1800

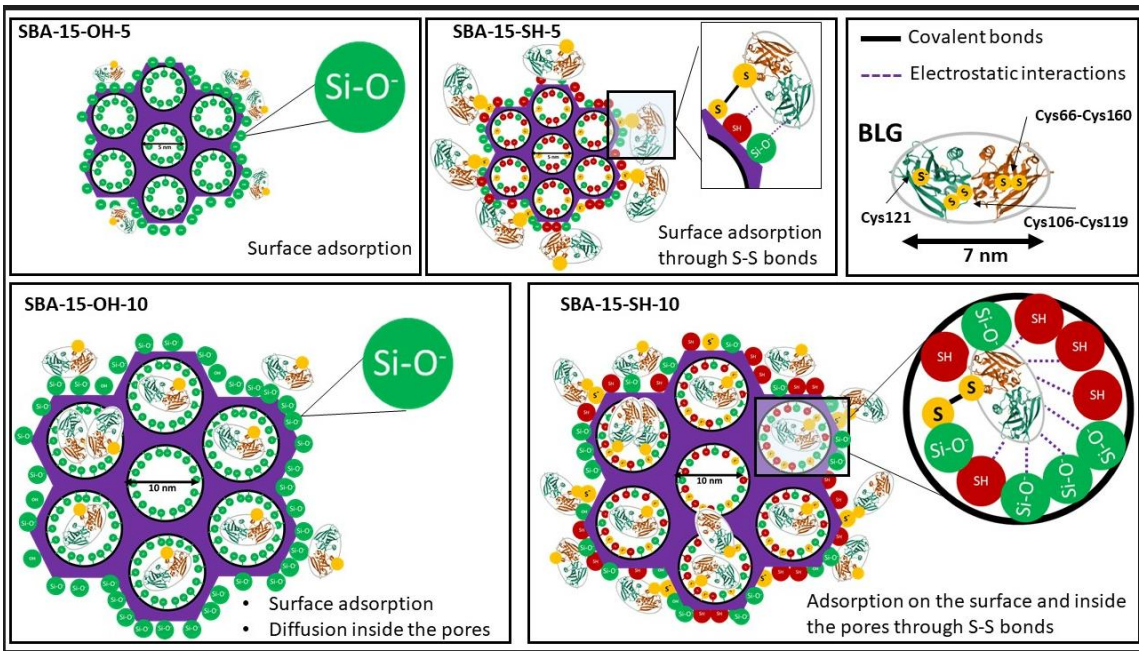

Figure 10. Illustrative scheme of the cooperative adsorption mechanism between a BLG protein and the active adsorption sites onto SBA-15-OH-10, SBA-15-OH-5, SBA-15-SH-10 and SBA-15-SH-5 adsorbents.